



Petrogenesis of Eocene calc-alkaline magmatism at Electric Peak and Sepulcher Mountain, Absaroka Volcanic Province, Montana and Wyoming
by Charles Roger Lindsay

A thesis submitted in partial fulfillment of the requirements for the degree of Master of Science in Earth Sciences
Montana State University
© Copyright by Charles Roger Lindsay (2002)

Abstract:

Electric Peak and Sepulcher Mountain represent the well-exposed intrusive and extrusive components of an early Eocene eruptive center in the Absaroka volcanic province of Montana and Wyoming. Geological field relationships, petrographic analysis, and mineral and whole rock geochemical compositions were used to investigate the petrogenesis of this eruptive center. The Electric Peak stock has an outcrop area of $\sim 1 \text{ km}^3$ and consists of six intrusive phases ranging in composition from quartz diorite to granite, representing multiple intrusions of compositionally distinct magmas. Stratigraphic constraints and Al-in-hornblende geobarometry indicate that these magmas stalled and solidified at a depth of $\sim 3 \text{ km}$. Lava flows and dikes at Sepulcher Mountain are basaltic-andesitic to rhyolitic in composition and silicic rocks are peripheral to mafic rocks. Collectively, intrusive and extrusive rocks represent a medium- to high-K, calc-alkaline, comagmatic suite. Important geochemical characteristics of these rocks include high Ni and Cr concentrations in andesitic and dacitic rocks, lower rare earth element concentrations in evolved rocks relative to more mafic rocks, non-uniform Sr and Nd isotopic ratios, and strong relative depletions in high field strength elements relative to large ion lithophile elements. Although petrographic evidence permissive of magma mixing is limited, quantitative petrogenetic modeling demonstrates that intermediate composition rocks are hybrids formed by mixing of variably fractionated and contaminated mantle-derived mafic magmas with diverse composition crustal-derived silicic magmas and their differentiates. Chemical compositions indicate that mafic magmas were derived from ancient, enriched lithospheric mantle and that silicic magmas represent partial melts of amphibolitic crust leaving restites with variable modal mineralogy. The significance of these results is that a considerable crustal component was involved in generating Eocene calc-alkaline magmas in the Absaroka volcanic province.

PETROGENESIS OF EOCENE CALC-ALKALINE MAGMATISM AT ELECTRIC
PEAK AND SEPULCHER MOUNTAIN, ABSAROKA VOLCANIC PROVINCE,
MONTANA AND WYOMING

by

Charles Roger Lindsay

A thesis submitted in partial fulfillment
of the requirements for the degree

of

Master of Science

in

Earth Sciences

MONTANA STATE UNIVERSITY
Bozeman, Montana

January, 2002

© COPYRIGHT

by

Charles Roger Lindsay

2002

All Rights Reserved

N378
26448

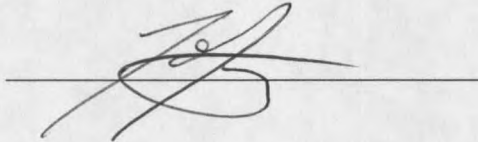
APPROVAL

of a thesis submitted by

Charles Roger Lindsay

This thesis has been read by each member of the thesis committee and has been found to be satisfactory regarding content, English usage, format, citations, bibliographic style, and consistency, and is ready for submission to the College of Graduate Studies.

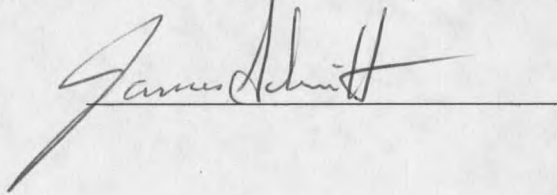
Dr. Todd C. Feeley



1/28/02
Date

Approved for the Department of Earth Sciences

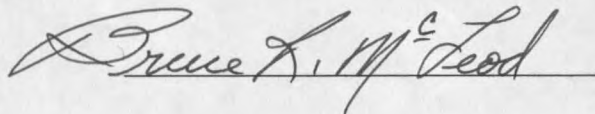
Dr. James G. Schmitt



1/28/02
Date

Approved for the College of Graduate Studies

Dr. Bruce McLeod



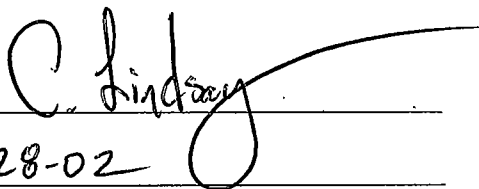
1-28-02
Date

STATEMENT OF PERMISSION TO USE

In presenting this thesis in partial fulfillment of the requirements for a master's degree at Montana State University, I agree that the Library shall make it available to borrowers under the rules of the Library.

If I have indicated my intention to copyright this thesis by including a copyright notice page, copying is allowable only for scholarly purposes, consistent with "fair use" as prescribed in the U.S. Copyright Law. Requests for permission for extended quotation from or reproduction of this thesis in whole or in parts may be granted only by the copyright holder.

Signature

A handwritten signature in cursive script that reads "C. Lindsay". The signature is written over a horizontal line.

Date

1-28-02

ACKNOWLEDGMENTS

The National Science Foundation, the Geological Society of America, and Sigma-Xi Grants-in-Aid of Research generously provided support for this project. Thank you also to the Department of Earth Sciences at Montana State University and the Barry C. Bishop Scholarship for Mountain Research for additional funding. The Radiation Center at Oregon State University kindly provided the instrumental neutron activation analyses. Thank you to Roger Nielson and François Bussy for assistance with the electron microprobe. I thank Anita Varley and Kerry Gunther for their assistance and permission to conduct fieldwork in Yellowstone National Park. I am indebted to Alan Swanson for his able and cheerful assistance in the field despite thunderstorms, mosquitoes, and grizzly bears. Special thanks to Dr. David Blackwell, Dr. Gordon G. Goles, Dr. Edward Taylor, and Dr. Anita Grunder for inspiration. Dr. David Egglar, Dr. B. Carter Hearn, and Dr. Margaret Hiza provided valuable insight and thoughtful discussion. I thank Cal Ruleman and Dr. Tom Kalakay for stimulating discussions and support during difficult times. Thank you Eric Hammond for listening and believing. Thank you Grace Winer for taking care of me. I thank my committee members, Dr. Jim Schmitt and Dr. Dave Mogk, for their large commitment of both time and resources. I thank my advisor Dr. Todd Feeley for his unwavering support and patience; your advice and guidance have helped me grow as a student, teacher, and scientist. Thank you Katie Johnson –for everything. I thank my parents for their support and encouragement. I thank my grandmother for the curiosity that she inspired within me.

TABLE OF CONTENTS

1. INTRODUCTION.....	1
Significance of Eocene Magmatism in the Northern Cordillera.....	3
2. GEOLOGIC SETTING.....	8
Tectonic Setting.....	8
Physical Volcanology of the AVP.....	10
Across-Strike Geochemical Variations.....	12
Southern Gallatin Range.....	13
Electric Peak Stock.....	15
Sepulcher Mountain and Peripheral Volcanic Vents.....	21
Geological Relationships Between Intrusive and Extrusive Rocks.....	26
3. ANALYTICAL METHODS.....	28
4. PETROGRAPHY, MINERAL COMPOSITIONS, AND MAGMATIC INTENSIVE PARAMETERS.....	31
Petrography.....	31
Sepulcher Mountain and Peripheral Volcanic Vents.....	31
Electric Peak Stock.....	34
Mineral Compositions.....	37
Plagioclase Feldspar.....	38
Orthoclase Feldspar.....	42
Olivine.....	42
Clinopyroxene.....	43
Orthopyroxene.....	43
Amphibole.....	45
Biotite.....	49
Fe-Ti Oxides.....	50
Quartz.....	50
Crystallization Sequences.....	52
Disequilibria Textural Features.....	53
Magmatic Intensive Parameters.....	57
Aluminum-in-Hornblende Geobarometry of the Electric Peak Stock.....	57
Plagioclase-Hornblende Geothermometry of the Electric Peak Stock.....	59
Geobarometric Results.....	60
Fe-Ti Exchange Geothermometry of Sepulcher Mountain Dacites.....	63
Aluminum-in-Hornblende Geobarometry of Sepulcher Mountain Lavas.....	65
Pressure-Temperature Conditions.....	65

TABLE OF CONTENTS – CONTINUED

5. WHOLE ROCK CHEMICAL COMPOSITIONS.....	67
Major Elements	67
Trace Elements.....	70
Sr and Nd Isotopes.....	76
6. PETROGENESIS.....	80
Evidence for Magma Mixing	81
Constraints on Primary Magma Composition.....	84
Origin of Intermediate Composition Magmas	85
Origin of Silicic Magmas.....	88
Summary	94
7. DISCUSSION	95
Petrogenetic Model.....	95
Implications for the Origin of Magmas in the AVP	97
8. CONCLUSIONS.....	99
REFERENCES CITED	101
APPENDICES.....	115
APPENDIX A: SAMPLE LOCATIONS AND PETROGRAPHIC DESCRIPTIONS	116
APPENDIX B: FELDSPAR COMPOSITIONS.....	129
APPENDIX C: PYROXENE COMPOSITIONS	137
APPENDIX D: AMPHIBOLE COMPOSITIONS	140
APPENDIX E: MAGNETITE COMPOSITIONS.....	143
APPENDIX F: ILMENITE COMPOSTIONS.....	146
APPENDIX G: MAJOR AND TRACE ELEMENT CONCENTRATIONS OF EPSM ROCKS.....	149

TABLE OF CONTENTS – CONTINUED

APPENDIX H: MINERAL/MELT PARTITION COEFFICIENTS FOR BASALTIC AND BASALTIC-ANDESITIC MELTS USED IN AFC MODELING	152
APPENDIX I: MINERAL/MELT PARTITION COEFFICIENTS USED IN CRUSTAL MELTING MODELS.....	154

LIST OF TABLES

Table	Page
1. Representative feldspar compositions	40
2. Representative clinopyroxene compositions	44
3. Representative orthopyroxene compositions	46
4. Representative amphibole compositions	46
5. Representative magnetite compositions	51
6. Representative ilmenite compositions	51
7. Average composition of coexisting Fe-Ti oxides and calculated pre-eruptive temperatures for two Sepulcher Mountain dacites	64
8. Major and trace element concentrations for representative EPSM rocks	68
9. Sr and Nd isotopic compositions of representative EPSM rocks.....	77
10. Fractional crystallization model for dacitic and rhyolitic rocks	93

LIST OF FIGURES

Figure	Page
1. The northwestern United States and Canadian Cordillera showing the location of early- to middle-Eocene volcanic fields	2
2. Generalized geologic map of the Absaroka volcanic province showing spatial extent of the major stratigraphic divisions of the Absaroka Volcanic Supergroup and location of the Electric Peak – Sepulcher Mountain eruptive center	11
3. Geologic map of a portion of northwestern Yellowstone National Park.	14
4. Two of the three main intrusive bodies of the Electric Peak stock viewed from the south	16
5. Geologic map of the Electric Peak stock	18
6. IUGS modal classification of holocrystalline intrusive rocks from Electric Peak	20
7. The north ridge of Sepulcher Mountain viewed from the Reese Creek drainage	23
8. Generalized stratigraphic sections for volcanic sequences at Sepulcher Mountain	25
9. Variation of modal abundances of phenocryst phases in extrusive rocks from Sepulcher Mountain versus whole rock SiO ₂ wt%	32
10. Medium-grained, holocrystalline, inequigranular texture representative of microporphyries from the Electric Peak stock	34
11. Variation of modal abundances of mineral phases in intrusive rocks from Electric Peak versus whole rock SiO ₂	36

LIST OF FIGURES – CONTINUED

12. Coarse-grained, holocrystalline hornblende gabbro inclusion from the base of the granodiorite phase of the Electric Peak stock.....	37
13. Plagioclase phenocryst exhibiting a euhedral rim mantling a spongy cellular core.....	39
14. Ternary projection of feldspar compositions of extrusive rocks from Sepulcher Mountain and intrusive rocks from Electric Peak grouped by whole rock compositional series	41
15. Ternary projection and classification of pyroxenes in extrusive rocks from Sepulcher Mountain	44
16. Eustructural amphibole with low structural integrity in a microporphyry from the Electric Peak stock.....	48
17. Plot of total Aluminum versus tetrahedral Aluminum in hornblende	48
18. Classification of calcic-amphiboles.....	49
19. Ternary projections of Fe-Ti oxide compositions from representative extrusive rocks from Sepulcher Mountain	52
20. Rounded anhedral amphibole phenocryst exhibiting a heavily oxidized rim and thin corona composed of plagioclase, clinopyroxene, and Fe-Ti oxides	54
21. Euhedral plagioclase phenocryst exhibiting a thin, sieved margin and spongy cellular core.....	54
22. Holocrystalline dacitic inclusion within a fine-grained, hypocrystalline andesitic dike	55
23. Disaggregating holocrystalline dacitic inclusion in dike SM9814	55
24. Calculated crystallization pressures for the Electric Peak stock using various Aluminum-in-hornblende barometers.....	61

LIST OF FIGURES – CONTINUED

25. Pressure-temperature diagram showing some of the anhydrous and water-saturated solidus and liquidus curves for granite and basalt.....	66
26. Major element variation diagrams for EPSM rocks	69
27. Trace element variation diagrams for EPSM rocks.....	71
28. Trace element concentrations of EPSM rocks normalized to the composition of chondritic meteorites and plotted from left to right in order of increasing compatibility in a small fraction melt of the mantle	73
29. Chondrite-normalized rare earth element patterns for EPSM rocks.....	75
30. Comparison of $^{143}\text{Nd}/^{144}\text{Nd}_i$ and $^{87}\text{Sr}/^{86}\text{Sr}_i$ compositions of EPSM rocks with: modern subduction-related basalts, the mantle array, mafic to silicic lower-crustal xenoliths from the Highwood Mountains, Montana, Archean granitoids and orthoamphibolites from the Beartooth Mountains, Montana.....	78
31. Petrogenetic model for the origin of compositional diversity at EPSM.....	83
32. Calculated assimilation-fractional crystallization models for $^{87}\text{Sr}/^{86}\text{Sr}_i$ and $^{143}\text{Nd}/^{144}\text{Nd}_i$	88
33. Results of crustal melting models for type 2 and type 3 dacitic rocks	92
34. Schematic petrogenetic model for the origin of compositional diversity of calc-alkaline magmas at Electric Peak and Sepulcher Mountain	96

ABSTRACT

Electric Peak and Sepulcher Mountain represent the well-exposed intrusive and extrusive components of an early Eocene eruptive center in the Absaroka volcanic province of Montana and Wyoming. Geological field relationships, petrographic analysis, and mineral and whole rock geochemical compositions were used to investigate the petrogenesis of this eruptive center. The Electric Peak stock has an outcrop area of $\sim 1\text{km}^3$ and consists of six intrusive phases ranging in composition from quartz diorite to granite, representing multiple intrusions of compositionally distinct magmas. Stratigraphic constraints and Al-in-hornblende geobarometry indicate that these magmas stalled and solidified at a depth of ~ 3 km. Lava flows and dikes at Sepulcher Mountain are basaltic-andesitic to rhyolitic in composition and silicic rocks are peripheral to mafic rocks. Collectively, intrusive and extrusive rocks represent a medium- to high-K, calc-alkaline, comagmatic suite. Important geochemical characteristics of these rocks include high Ni and Cr concentrations in andesitic and dacitic rocks, lower rare earth element concentrations in evolved rocks relative to more mafic rocks, non-uniform Sr and Nd isotopic ratios, and strong relative depletions in high field strength elements relative to large ion lithophile elements. Although petrographic evidence permissive of magma mixing is limited, quantitative petrogenetic modeling demonstrates that intermediate composition rocks are hybrids formed by mixing of variably fractionated and contaminated mantle-derived mafic magmas with diverse composition crustal-derived silicic magmas and their differentiates. Chemical compositions indicate that mafic magmas were derived from ancient, enriched lithospheric mantle and that silicic magmas represent partial melts of amphibolitic crust leaving restites with variable modal mineralogy. The significance of these results is that a considerable crustal component was involved in generating Eocene calc-alkaline magmas in the Absaroka volcanic province.

CHAPTER 1

INTRODUCTION

A widespread magmatic event affected northwestern North America during the Eocene, emplacing several large igneous provinces throughout the Cordillera and adjacent foreland (Figure 1). The genesis of this magmatic activity remains poorly understood as reflected by the numerous contrasting models that have been proposed to account for it (e.g. Lipman and Glazner, 1991; Lipman, 1992). As one of the largest volcanic fields in this region, the Absaroka volcanic province (AVP; Figure 1) is similarly difficult to place in a proper tectonomagmatic context. Understanding the magmatic processes involved in the evolution of individual eruptive centers is critical to unraveling the origin of the volcanic field as a whole. Therefore, this study investigates the petrogenesis of Electric Peak and Sepulcher Mountain, the well-exposed intrusive and extrusive components of a moderate-volume, calc-alkaline, early Eocene eruptive center in the AVP. Specifically, the goals of this study are to (1) document the compositional ranges of extrusive and intrusive rocks present; (2) characterize the relationship between intrusive rocks at Electric Peak and extrusive rocks at Sepulcher Mountain; and (3) evaluate the possible roles of different petrogenetic processes in producing the compositional diversity of these rocks.

Electric Peak and Sepulcher Mountain were chosen for this study for two reasons. First, there are few contemporary petrologic studies of calc-alkaline eruptive centers in the AVP (Hiza, 1999; Feeley et al., *in press*). Second, intrusive bodies at Electric Peak

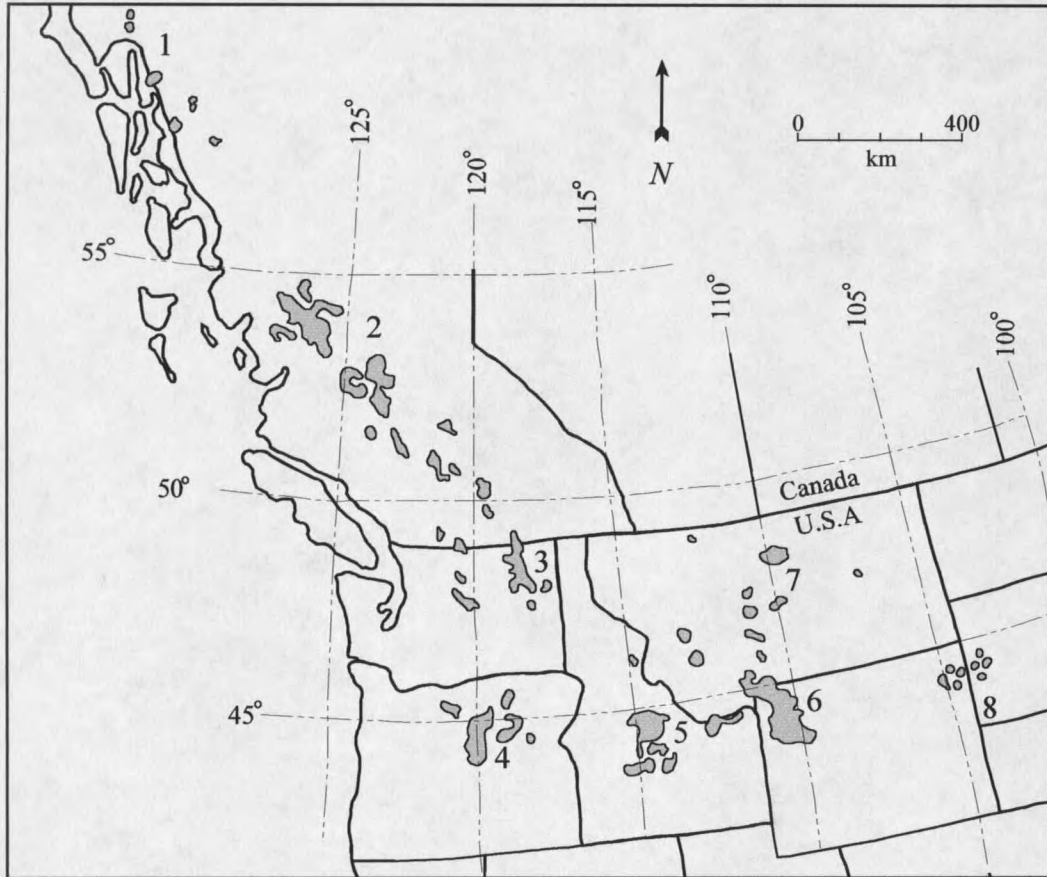


Figure 1. The northwestern United States and Canadian Cordillera showing the location of early- to middle-Eocene volcanic fields (adapted from Chadwick, 1985; Armstrong, 1988; Dudas, 1991; Norman and Mertzman, 1991; Luedke, 1994; and Morris et al., 2000). Numbers refer to: 1. Sloko volcanic province, 2. Francois Lake igneous complex, 3. Colville igneous complex, 4. Clarno volcanics, 5. Challis volcanic province, 6. Absaroka volcanic province, 7. Montana alkalic province, 8. Black Hills-Bear Lodge Mountains igneous centers.

are thought to represent subvolcanic intrusive bodies related to extrusive rocks at Sepulcher Mountain (Iddings, 1891; Smedes and Prostka, 1972), but no genetic relationship has been established, and thus they have never been formally included in the Absaroka Volcanic Supergroup (Smedes and Prostka, 1972).

Significance of Eocene Magmatism in the Northern Cordillera

Eocene igneous provinces are distributed throughout the northern Rocky Mountains forming a belt that stretches from southern Yukon to Wyoming. This belt is relatively narrow in British Columbia (~70-300 km) and is diffuse (~1400 km) in the northwestern United States between 43° and 48° north latitude (Figure 1). Collectively, these igneous provinces were originally interpreted as an early Tertiary magmatic arc (Lipman et al., 1972; Coney and Reynolds, 1977), analogous to those formed above modern subduction zones (e.g. the Cascade and Andean arcs). This "arc" is sometimes referred to as the "Challis Arc", although in this study it is termed the Eocene magmatic belt.

Two notable features of the Eocene magmatic belt are its width between 43° and 48° north latitude and the number of discrete igneous provinces located within this region (Figure 1). Three large (>15,000 km³), roughly contemporaneous volcanic fields, the Clarno (~47-34 Ma; Vance, 1988; Urbanczyk and Lilligren, 1990), Challis (~51-40 Ma; Norman and Mertzman, 1991), and Absaroka (~55-38 Ma; Hiza, 1999; Lindsay et al., 2000; Feeley et al., *in press*) fields, are located across this region. Four smaller areas situated across this region were also strongly affected by Eocene magmatism. These include the Colville igneous complex, Montana alkalic province, and the Black Hills-

Bear Lodge Mountains igneous centers. Petrologic investigations of these igneous provinces over the last four decades have documented the chemical compositions of rocks present, allowing for general comparison.

Rocks with either calc-alkaline or alkaline-potassic geochemical affinities characterize Eocene igneous rocks across this region. Calc-alkaline rocks are volumetrically dominant and include intermediate (~54-65 wt % SiO₂), high-alumina (>15 wt % Al₂O₃), and low- to high-K (LeMaitre et al., 1989) compositions. These compositions are typical of rocks documented at the Challis (Norman and Mertzman, 1991) and Absaroka (Chadwick, 1970) volcanic fields as well as at the Colville igneous complex (Morris et al., 2000). Alkaline-potassic rocks are generally strongly silica undersaturated (Ne-normative, ≤30%), potassic (K₂O/Na₂O ≈1.0-6.0), and predominately mafic, compositions typical of rocks documented across the Montana alkalic province and at the Black Hills-Bear Lodge Mountains igneous centers (Jenner, 1989).

Lipman et al. (1972) first recognized that the distribution of calc-alkaline and alkaline-potassic rocks across this region reflects generally increasing K₂O contents eastward across the region. Although rocks from a specific igneous province generally exhibit either calc-alkaline or alkaline-potassic affinities, both types also occur in close proximity at the Crazy Mountains in the Montana alkalic province (Dudás, 1991) and at the Independence volcano in the AVP (Meen and Egger, 1987). In addition to exhibiting either calc-alkaline or alkaline-potassic affinities, widely distributed igneous rocks from across the Eocene magmatic belt display remarkable chemical similarities to each other and to rocks found at modern volcanic arcs.

Striking features shared to some extent by both calc-alkaline and alkaline rocks from the Eocene magmatic province are high abundances of large ion lithophile elements (LILE) relative to abundances of high field strength elements (HFSE). For example, extreme LILE abundances of Ba >1000 ppm, Sr >450 ppm, and Rb >60 ppm and HFSE abundances of Zr <200 ppm, Nb <20 ppm, Ta <2.0 ppm, and Ti <6000 ppm are typical of rocks from the Colville igneous complex, (Morris et al., 2000), Challis volcanic field (Norman and Mertzman, 1991), Absaroka volcanic province (Meen, 1987), and Montana alkalic province (Dudás, 1991). Enrichment in LILE relative to HFSE is considered a characteristic geochemical signature of arc-related igneous rocks (Pearce and Norry, 1979; Perfit et al., 1981). Specifically, values of Ba/Ta >450 and Ba/Nb >25 are considered diagnostic of subduction-related magmatism (Gill, 1981). In light of these parameters, a cursory interpretation of these compositions might suggest the involvement of a subduction-related component.

Petrogenetic hypotheses regarding the origin of these igneous rocks are both varied and controversial, and strikingly different tectonomagmatic models have been proposed for their origin. Recognition of the predominately calc-alkaline nature of rocks emplaced contemporaneously with subduction of the Farallon Plate beneath western North America led early workers to develop models that related these rocks to subduction. Eastward increasing potassium contents across the magmatic belt were thought to represent increasing depth to the subducting Farallon Plate and, therefore, increasing interaction of subduction-related magmas with continental crust (K-h relationship of Dickinson and Hatherton, 1967). Lipman et al. (1971) interpreted the changing compositions of rocks and distribution of igneous activity across the belt in

relation to evolving subduction geometry between the North American and Farallon Plate and suggested that an "imbricate" double subduction zone was responsible for producing arc-like magmatism far inland from the Eocene trench. Further research modified this hypothesis, suggesting that changing plate convergence rates caused the dip of the subducted slab to shift from steep to shallow angles, resulting in temporally shifting loci of arc-like magmatism across a broad region (Bird, 1984; Ward, 1995). Eocene calc-alkaline and alkaline-potassic rocks from the Crazy and Highwood Mountains of the Montana alkalic province are currently interpreted to represent subduction-related magmas (O'Brien et al., 1991; du Bray and Harlan, 1996).

Other studies, although acknowledging that Eocene igneous rocks exhibit a "subduction-related geochemical signature", recognize a close spatial and temporal association between magmatism and large-scale crustal extension. This relationship is well documented at the Challis volcanic field (Norman and Mertzman, 1991) and Colville igneous complex (Morris et al., 2000) and has also been proposed for the AVP (Hiza, 1999). Petrogenetic models developed for these regions suggest that regional extension led to consequent decompression partial melting of the upper mantle and lower crust. The arc-like geochemical signature is interpreted as being inherited by Eocene magmas through interaction with, or derivation from, lithospheric mantle (Dudás, 1991) and continental crust (Morris et al., 2000) that was chemically "enriched" through pre-Eocene subduction-related magmatism. Alternatively, some researchers argue that Eocene magmatism across this region cannot be explained by simple subduction or extension related models and suggest that it may not be possible to identify a single causative melt-generation process or simple tectonomagmatic setting for Eocene

magmatism in northwestern North America (Meen and Eggler, 1987; Dudás, 1991; Irving and O'Brien, 1991; MacDonald et al., 1992).

The compositional significance and origin of Eocene magmatic rocks in the AVP remain poorly understood. One of the outstanding problems in deciphering the regional significance of the AVP is that petrologic data have been obtained from only a small fraction of the magmatic rocks exposed. Most previous studies have concentrated on mineralized areas and nearly all geochemical data is based on small sets of major-element analyses from widely separated localities (Chadwick, 1970; La Pointe, 1977; Nelson et al., 1980). Thus, the relative contributions of mantle, crustal, and potentially subducted sources to parental magmas and their subsequent differentiation processes are not well known. This study presents new information on the petrogenesis of a calc-alkaline magmatic center in the AVP and contributes to studies whose ultimate goal is to better understand the origin and tectonic significance of this large-scale Eocene magmatic event.

CHAPTER 2

GEOLOGIC SETTING

Tectonic Setting

The AVP is bordered on the west by the Yellowstone Plateau, on the northwest by the Madison Range, on the northeast by the Beartooth Mountains, on the east by the Bighorn Basin, and on the south by the Wind River Basin. The volcanic province occupies the Absaroka basin, a shallow Laramide foreland basin (Sundell, 1993) that formed concurrently with surrounding basement-cored uplifts exposed in the Washakie, Gallatin-Madison, and Beartooth mountain ranges. The majority of these uplifts experienced episodic contractional deformation from late Cretaceous through middle Eocene time (Schmidt and Garihan, 1983; Winterfield and Conrad, 1983). The AVP rests unconformably on deformed Paleozoic to Mesozoic carbonate and clastic sedimentary strata and on high-grade metamorphic and igneous rocks of the Wyoming Province, an Archean granite-gneiss craton that underlies much of Wyoming, Montana, and southeastern Idaho. Seismic refraction studies indicate that the crust beneath the AVP at present is ~45-50 km thick (Prodehl and Lipman, 1989) and lithospheric thickness is estimated to be at least 170 km thick based on the presence of a weak low-velocity zone at 170-225 km depth (Iyer and Hitchcock, 1989). Although the composition of the deep crust beneath the AVP is poorly constrained, an amphibolitic to granulitic lower-crust is inferred through geochemical evidence (Meen and Eggler, 1989) and xenolith geothermobarometry (Joswiak, 1992).

Regional extension associated with crustal thinning and development of metamorphic core complexes occurred during the early-to-mid Eocene in northeastern Washington (Morris and Hooper, 1997), north-central Idaho (Wust, 1986; Janecke, 1992; Janecke and Snee, 1993), and westernmost Montana (Foster and Fanning, 1997). Although contemporaneous with magmatism in the AVP, little evidence is documented for major Eocene extensional faulting within or directly adjacent to the AVP. Both listric and normal faults have been recognized and mapped across the AVP, but they are not acknowledged as products of regional extension (Montagne and Chadwick, 1982; Sundell, 1993). It has also been suggested that the Heart Mountain detachment may be associated with regional extensional faulting (Hiza, 1999), but there is little conclusive evidence to support this relationship. The Heart Mountain detachment is a shallow-rooted, bedding-parallel, low-angle normal fault that accommodated transport of the hanging wall for a distance of 50 km or more (Hauge, 1993). It appears to represent a structure associated with large-scale, eastward-directed, gravitational sliding of a growing volcanic highland (Hauge, 1985) and not regional crustal extension.

Magmatism in the AVP occurred between 55 and 38 Ma (Hiza, 1999; Lindsay et al., 2000; Feeley et al., *in press*), apparently during a transitional period in the tectonic framework of the northern Rocky Mountains. The earliest eruptions occurred directly after, but possibly overlapping with the last phases of Sevier- and Laramide-style contractional deformation (Love et al., 1975; Sundell, 1993). Magmatism also coincided with the onset of regional crustal extension in the northern Rocky Mountains directly west of the AVP (Burchfiel et al., 1992; Janecke and Snee, 1993; Foster and Fanning,

1997). Thus, magmatism in the AVP occurred during period critical to understanding the tectonomagmatic framework of the northern Cordillera in the early Tertiary period.

Physical Volcanology of the AVP

Encompassing an area of approximately 23,000 km² with a maximum thickness of 1500 m, the AVP is one of the most voluminous Eocene volcanic fields in the northern Cordillera (Steven et al., 1972). The inferred depositional setting for the AVP is an approximately 90 km wide belt of large stratovolcanoes, shield volcanoes, and dike swarms flanked by coalescing alluvial aprons (Sundell, 1993). Volcaniclastic rocks are volumetrically dominant and include volcaniclastic sandstone, siltstone, claystone, conglomerate, and breccia (Smedes and Prostka, 1972). Intercalated primary volcanic rocks increase in abundance near eruptive centers and include effusive lava flows, flow breccias, and domes as well as pyroclastic flow and fall deposits. Hypabyssal intrusive bodies are common at many of the eruptive centers and include dikes, sills, ring dikes, cone sheets, plugs, stocks, and laccoliths (Parsons, 1969).

Smedes and Prostka (1972) defined the Absaroka Volcanic Supergroup to include all volcanic rocks within the AVP as well as associated outliers erupted or deposited during the Eocene. They defined three stratigraphic divisions: the Washburn, Sunlight, and Thorofare groups. Rocks exposed at Sepulcher Mountain represent the type section for the Sepulcher Formation, the western member of the Washburn Group. The aerial distribution of these groups (Figure 2) and stratigraphic divisions are, however, currently under revision (e.g. Sundell and Eaton, 1982; Hiza, 1999).

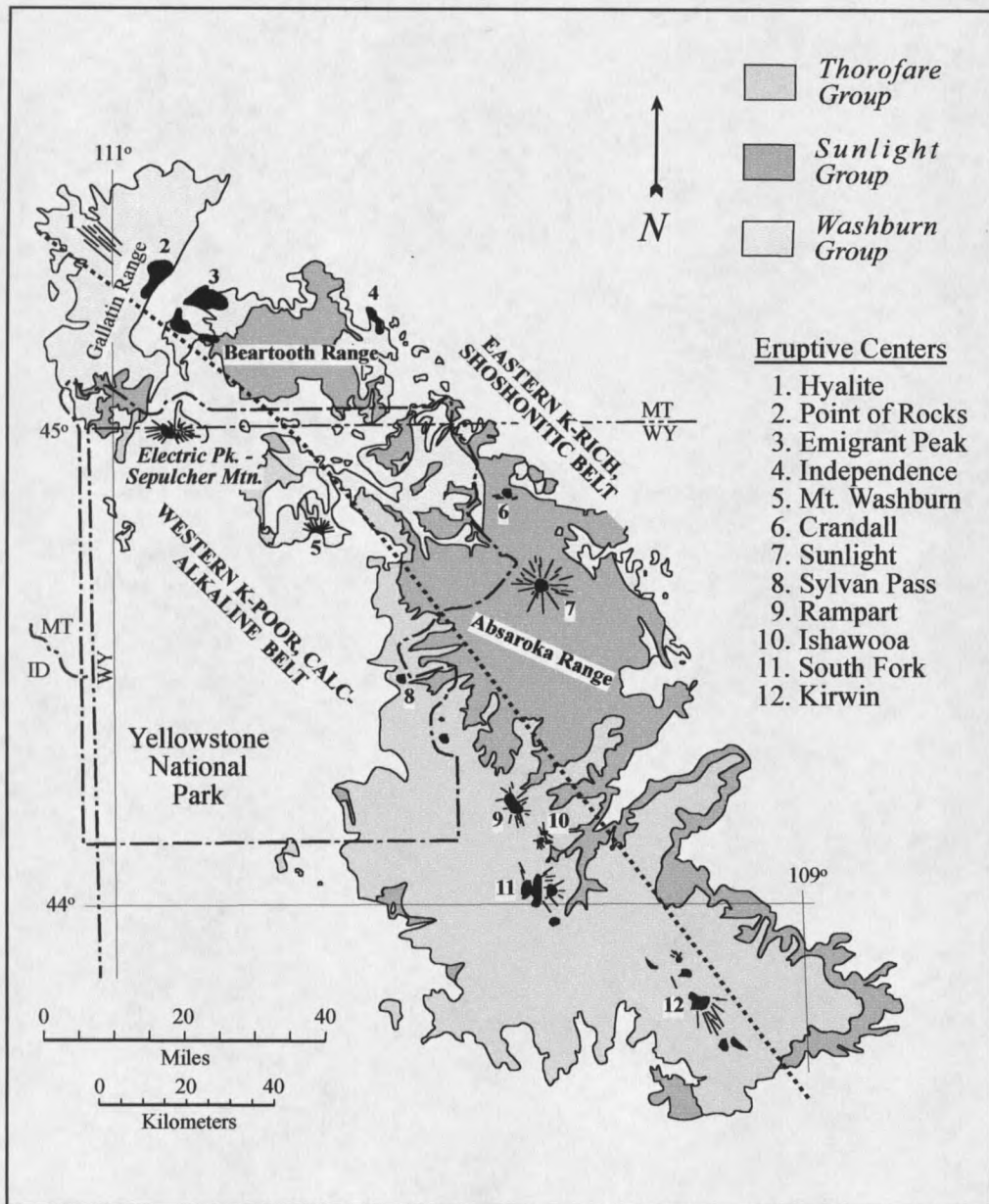


Figure 2. Generalized geologic map of the Absaroka volcanic province showing spatial extent of the major stratigraphic divisions of the Absaroka Volcanic Supergroup (modified from Smedes and Prostka, 1972; Chadwick, 1970) and location of the Electric Peak - Sepulcher Mountain eruptive center. Other eruptive centers discussed in the text are numbered for reference. Thick dashed line shows the approximate division between western potassium-poor and eastern potassium-rich belts (after Chadwick, 1970). Single dot-dashed line is the boundary of Yellowstone National Park.

Eruptive styles within the AVP were varied and are represented by Plinian airfall deposits (Sundell and Eaton, 1982), Hawaiian-style dike-fed lava flows and lava lakes (Nelson and Pierce, 1968), as well as deposits from Vesuvian-, Strombolian-, and Pelean-style eruptions (Wilson, 1964; Rubel, 1971; LaPointe, 1977). In addition, the Castle Rocks "chaos" is interpreted to be the deposit of a stratovolcano sector collapse that was one hundred times larger than that of the 1980 Mt. St. Helens eruption (Sundell, 1985). Although significantly eroded, edifice types likely included composite cones, shield volcanoes, silicic domes, small Mt. Mazama-sized calderas, and dike swarms. Paleorelief was likely greater than 3,000 m between the highest terrain (stratovolcanoes) and adjacent lowlands (alluvial aprons) based on compositional and morphological differences in fossil fauna and flora (Fritz, 1982; Yuretich, 1984).

Across-Strike Geochemical Variations

Thirteen distinct eruptive centers are presently recognized in the AVP and are aligned along two sub-parallel belts (Figure 2). Chadwick (1970) interpreted these lineaments as Precambrian structures that were reactivated during the Laramide Orogeny. On the basis of major element compositions from ~50 rocks from nine eruptive centers, Chadwick (1970) demonstrated that the two sub-parallel belts of eruptive centers exhibit significant compositional differences with respect to potassium content and differentiated a western "K-poor" calc-alkaline belt and an eastern "K-rich" shoshonitic belt (Figure 2). These across-strike variations in potassium content are similar to those observed at many subduction-related volcanic arcs (e.g. Gill, 1981; Tatsumi and Eggins, 1995) although the petrogenetic origin of these variations in the AVP is unclear.

Southern Gallatin Range

Electric Peak and Sepulcher Mountain (EPSM), a western-belt, calc-alkaline eruptive center, is located in the northwest corner of the AVP (Figure 2). Samples for this study were collected from an area bound on the northwest by the Yellowstone River, on the east by the North Entrance Road, to the south by the North Fork of the Gardner River, and on the west by $\sim 111^{\circ}52'$ west longitude (Figure 3). Although the region is semi-arid, bedrock geology is only moderately exposed at lower elevations due to extensive landslide deposits in both Eocene volcanic and Cretaceous sedimentary strata. Eocene igneous rocks are well exposed through late Tertiary to Quaternary normal faulting and Pleistocene glacial erosion at higher elevations on Electric Peak and Sepulcher Mountain.

The dominant structural feature in the area is the north-to-south oriented east Gallatin-Reese Creek fault system, represented by a 600 m fault scarp (Figure 3). The Reese Creek fault separates Electric Peak from Sepulcher Mountain and exhibits greater than 1200 m of stratigraphic displacement of Paleozoic and Mesozoic sedimentary strata (Pierce et al., 1991). The uplifted southern Gallatin Range footwall block consists of gently folded Paleozoic and Mesozoic carbonate and clastic sedimentary rocks that overlie Archean biotite-bearing gneissic granitoids. The sedimentary strata dip gently ($\sim 10^{\circ}$ - 20°) to the north-northeast exposing almost the entire stratigraphic section from the Cambrian Flathead Sandstone to the Late Cretaceous Landslide Creek Formation. Laccoliths, stocks, sills, and dikes intrude the sedimentary strata in the southern Gallatin Range. Consistent with the age relationships recognized by Iddings (1889), Ruppel

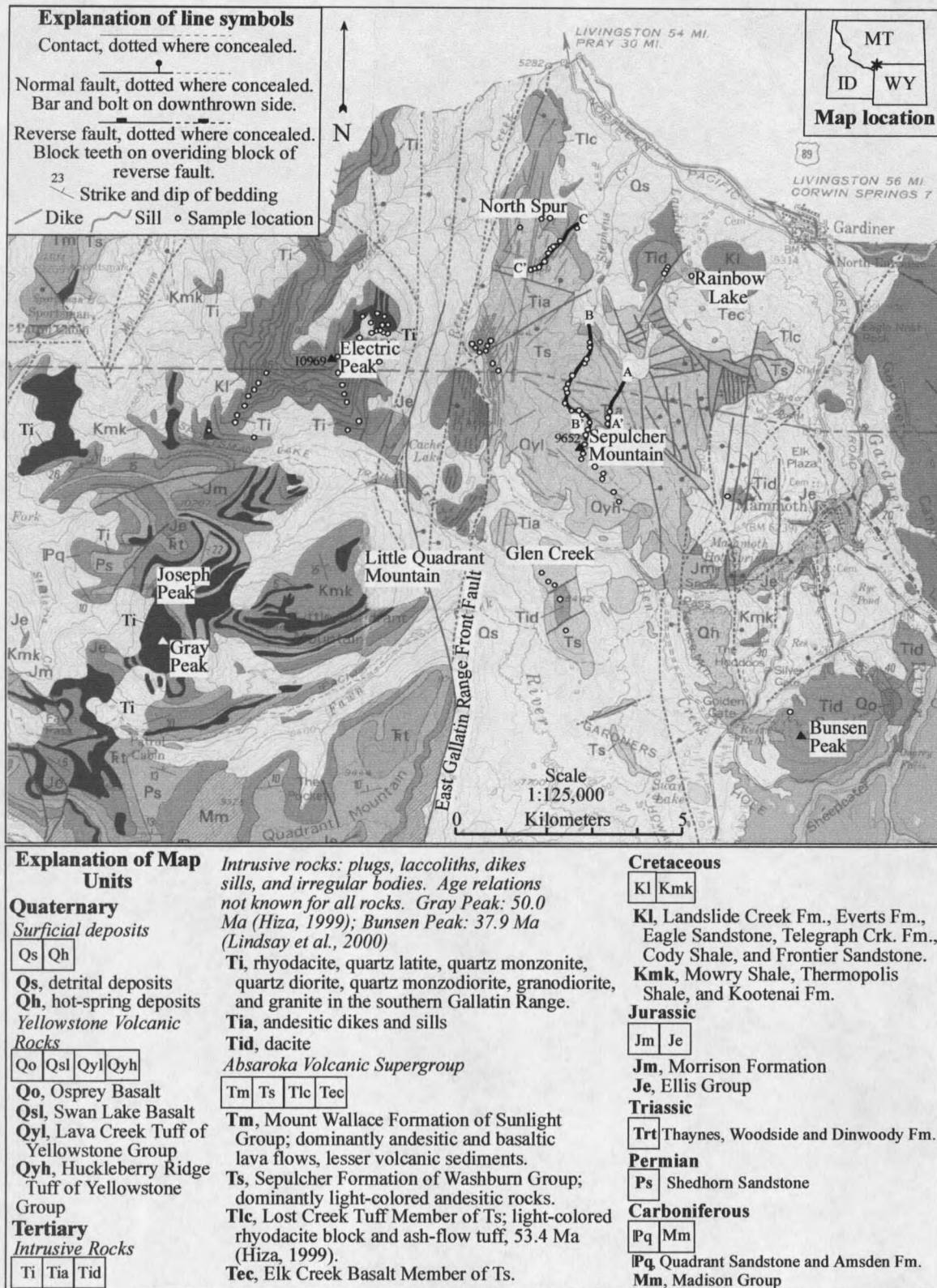


Figure 3. Geologic map of a portion of northwestern Yellowstone National Park (U.S.G.S., 1972). The locations of generalized stratigraphic sections for the volcanic sequence at Sepulcher Mountain are indicated with lines labeled: A-A', B-B', and C-C'.

(1972) suggests that there is a south-to-north age progression of intrusive activity in the southern Gallatin Range, with the Mt. Holmes stock in the southern end of the range being the oldest and the Electric Peak stock at the northern end being the youngest. However, both of these interpretations are based on often poorly exposed field relationships. Only the Gray Peak laccolith (Figure 3) has yielded a reliable radiometric age (50.00 ± 0.09 Ma; $^{40}\text{Ar}/^{39}\text{Ar}$ on biotite separate; Hiza, 1999).

Electric Peak Stock

Electric Peak is the highest point (3,342 m) on the 30 km long ridge that forms the southern Gallatin Range. It consists of predominately Cretaceous shallow marine clastic sedimentary rocks including the Frontier Sandstone, Cody Shale, Telegraph Creek Formation, and Eagle Sandstone. Numerous sills intrude these sedimentary rocks. The sills are typically 1-5 m thick, porphyritic, and dacitic in composition. They are characterized by phenocrysts of plagioclase feldspar, amphibole, and biotite and are pervasively altered, often appearing bleached. These sills radiate from the Gray Peak laccolith (Figure 3), located ~6 km southwest of Electric Peak (Ruppel, 1972). Ruppel (1972) estimates that the Cretaceous stratigraphic section in the northern part of the Southern Gallatin Range is doubled in thickness due to the large number of sills present. Collectively, the sills and sedimentary sequence at Electric Peak are faulted, crosscut, and weakly metamorphosed through contact with the Electric Peak stock that cores the peak.

The Electric Peak stock has an outcrop area of ~1 km³ and is pyramidal in shape. It is exposed in the walls of two glacial cirques on the east and northeast side of Electric Peak and on the dividing arête (Figure 4). A geologic map of the Electric Peak stock is



Figure 4. Two of the three main intrusive bodies of the Electric Peak stock viewed from the south. The darker wedge shaped body in the center foreground of the photograph is ~ 90 m in height and is composed of five intrusive phases ranging in composition from quartz diorite to granite. The darker knobs on the ridge in center midground of the photograph are smaller holocrystalline outcrops projecting from the roof of an intrusion probably similar in shape to the one in the foreground. Emigrant Peak, another early Eocene eruptive center in the Absaroka Volcanic Province, is visible on the skyline in the background of the photograph.

presented in Figure 5. Although the bulk of the stock is covered with talus, six intrusive phases are recognized: five holocrystalline phases of the stock and one hypocrySTALLINE phase represented by dikes. Collectively, the six intrusive phases represent a texturally and compositionally zoned, hypabyssal, small-volume stock.

Individual intrusive phases of the Electric Peak stock exhibit minor textural zonation. Silicic holocrystalline phases are typically fine- to medium-grained and intermediate composition holocrystalline phases are typically fine-grained. The deceptive coarse-grained appearance of holocrystalline rocks is due to the presence of abundant mafic and felsic glomerocrysts. Dikes are porphyritic, contain a hypocrySTALLINE groundmass, and are typically fine-to medium-grained. Chilled margins are present in both hypocrySTALLINE and holocrystalline phases with grain size decreasing within 0.10 m of intrusive contacts with country rock.

Intrusive phases of the Electric Peak stock display sharp, discordant contacts with the Cody Shale, Telegraph Creek Formation, and Eagle Sandstone. Contacts are typically narrow (<0.01 m), jagged, and discordant to sedimentary bedding. Sedimentary and metamorphic xenoliths are abundant along the margins of the intrusion. Shale and sandstone xenoliths are lithologically similar to Cretaceous sedimentary country rock (e.g. Cody Shale, Frontier Sandstone) and hornblende-plagioclase-garnet gneissic xenoliths are similar to Archean metamorphic lithologies exposed in Yankee Jim Canyon (~5 km north of the study area). Sedimentary and metamorphic xenoliths commonly exhibit sharp (<0.005 m) contacts with their intrusive host and are often surrounded by a thin (<0.01 m) concentration of leucocratic rock. Medium-to coarse-grained hornblende gabbro magmatic inclusions (0.005-0.10 m long-axis) are abundant at the base of one

granodiorite outcrop (EP9714) and are less abundant, but present, throughout all holocrystalline phases of the Electric Peak stock.

The Electric Peak stock exhibits considerable compositional diversity. Normalized modal compositions of samples from the Electric Peak Stock are plotted in Figure 6 (Streckeisen, 1979). Rocks from discrete intrusive bodies within the stock range compositionally from biotite-amphibole quartz diorite to amphibole-bearing biotite granite. A spatial pattern in the distribution of intrusive compositions is difficult to recognize, however, silicic phases appear to be peripheral to more intermediate phases (Figure 5). Individual intrusions of the Electric Peak stock do not exhibit mineralogical phase zoning but do exhibit mineralogical ratio zoning. The mafic- to felsic-mineral ratio generally increases slightly within 5 – 10 m of intrusive contacts. Contacts between individual intrusions range from sharp to diffuse but are always less than 0.10 m in width and are typically as sharp as 0.01 m.

The relatively sharp contacts between different intrusive phases and lack of significant compositional zonation (e.g. phase zoning) within individual intrusive phases indicate a composite origin for the stock. Textural and compositional zoning within the stock as a whole are thus not interpreted to represent the *in situ* differentiation of a single intrusion. Alternatively, these features likely resulted from multiple intrusions of diverse composition magma. The spatial distribution of compositions may be entirely random, the result of different magma density on emplacement, or the result of successive tapping of a deeper, temporally evolving magmatic system.

Intrusive rocks of the Electric Peak stock cut the numerous sills present at Electric Peak. The geologic map of Ruppel (1972) shows these sills as radiating from the Gray

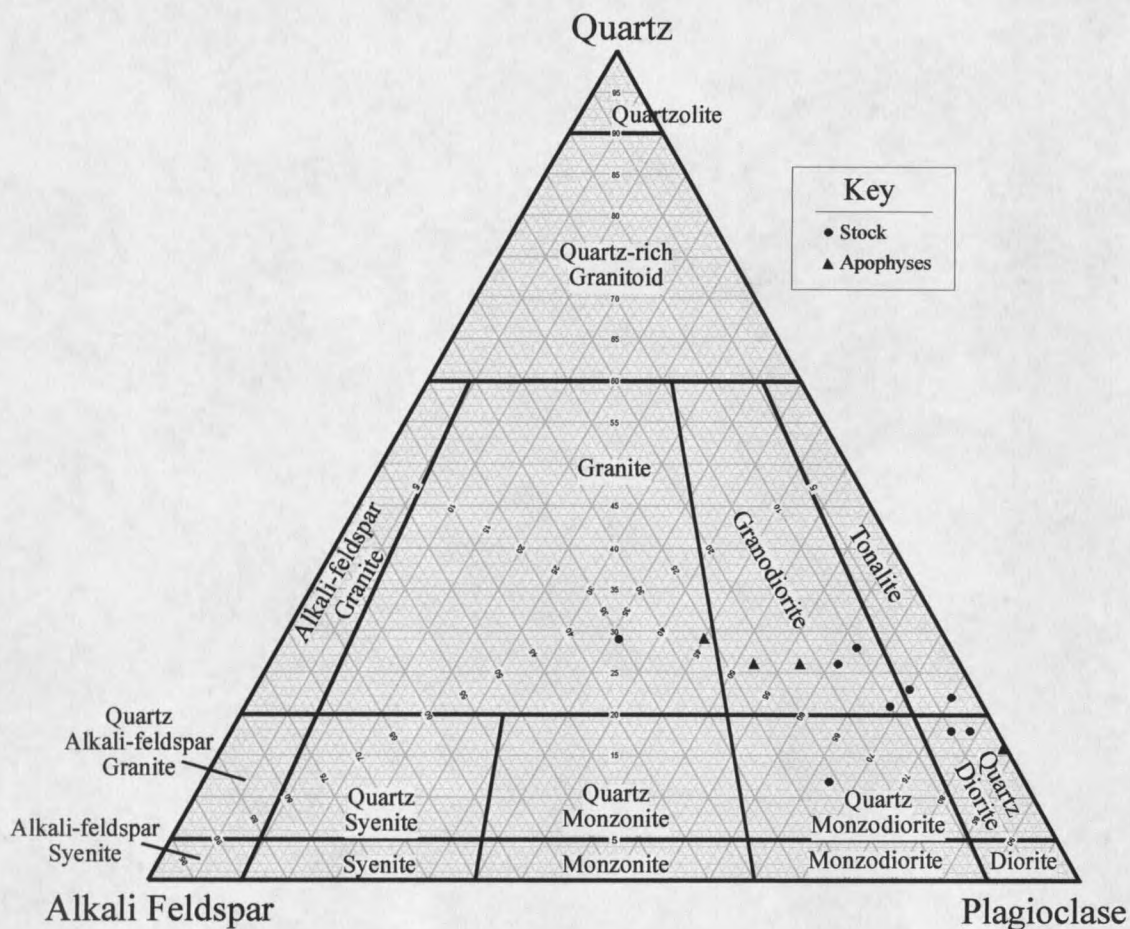


Figure 6. IUGS modal classification of holocrystalline intrusive rocks from Electric Peak (modified after Streckeisen, 1979). Circles represent samples from the Electric Peak stock, triangles represent samples from apophyses of this stock. Modal classifications of some samples ($n=7$) are qualitative as modal abundances of alkali feldspar were estimated in unstained thin sections.

Peak laccolith (Figure 3), which has been radiometrically dated by the $^{40}\text{Ar}/^{39}\text{Ar}$ method at 50.06 Ma (Hiza, 1999). This crosscutting relationship suggests that the Electric Peak stock is younger than 50.06 Ma. Age relationships within the Electric Peak stock are difficult to ascertain. Although crosscutting relationships are recognizable at individual outcrops, these relationships are entirely buried by talus between different outcrops of the Electric Peak Stock. Although tentative, cross-cutting age relationships recognized in the field were extrapolated to outcrops of similar composition. Intrusive activity began with emplacement of quartz diorite and was followed by intrusion of quartz monzodiorite, granodiorite, tonalite, and granite. Dikes crosscut the granite phase and are interpreted to represent the terminal stage of intrusive activity at Electric Peak.

Sub-solidus alteration is extensive at Electric Peak. Both sills emanating from the Gray Peak laccolith and dikes radiating from the Electric Peak stock exhibit pervasive sericitic alteration and secondary growth of calcite. Sills characteristically appear bleached, and plagioclase in these rocks is often completely replaced by sericite. Dikes are typically oxidized to a dark red color and exhibit secondary crystallization of calcite in vesicles, replacement of plagioclase by sericite, and replacement of both amphibole and biotite by chlorite. Holocrystalline intrusive phases are considerably less altered and extreme care was taken in the field to collect only fresh, unaltered samples.

Sepulcher Mountain and Peripheral Volcanic Vents

Volcanic rocks of the Sepulcher Formation are exposed along a structural low of the east Gallatin-Reese Creek fault system (Pierce et al., 1991; Figure 3). Primary volcanic rocks are abundant in this region and grade laterally eastwards into

volcaniclastic sedimentary rocks. Although a central vent region was not identified, the high concentration of primary volcanic rocks present at Sepulcher Mountain suggests that it represents the preserved remnant of an eroded volcanic edifice (Iddings, 1891; Smedes and Prostka; 1972).

The north side of Sepulcher Mountain consists of a vertical section of intercalated volcanic products, greater than 1000 m thick (Figure 7), which grade from basal epiclastic alluvial facies into an upper sequence of vent facies lava flows and flow breccias. Lava flows are horizontal to shallow dipping and dikes are abundant. Nearly complete stratigraphic sections of primary volcanic rocks are exposed at the cliffs above Stephens Creek (section A-A'; Figure 3), along the north ridge of Sepulcher Mountain (section B-B'; Figures 3 and 7), and at the north spur of Sepulcher Mountain (section C-C'; Figure 3). Primary volcanic rocks are also present at several small eruptive centers along Glen Creek (Figure 3), at a rhyodacite dome near Rainbow Lakes (Figure 3), and at Bunsen Peak, a rhyodacite plug five kilometers southwest of Sepulcher Mountain (Figure 3). Bunsen Peak, however, is significantly younger (37.9 Ma, $^{40}\text{Ar}/^{39}\text{Ar}$ on biotite separate) than other rocks present at Sepulcher Mountain and is thus not related (Lindsay et al., 2000).

The Sepulcher block and ash-flow tuff is exposed at the base of the north spur of Sepulcher Mountain (Figure 3). This tuff was included as part of a regional stratigraphic and geochronologic study by Hiza (1999) because it was originally considered to be part of the Lost Creek Tuff, a regional ash-flow tuff. $^{40}\text{Ar}/^{39}\text{Ar}$ dating of biotite from the Sepulcher block and ash-flow tuff yielded a disturbed spectrum caused by excess Argon. The maximum estimate for the age of this unit based on the disturbed spectrum is $53.36 \pm$



Figure 7. The North Ridge of Sepulcher Mountain viewed from the Reese Creek drainage. Approximately 900 vertical meters of roughly horizontal, intercalated eruptive products are visible in this photograph. The prominent buttness in the center of the photograph is capped by a two-pyroxene andesite lava flow ~15 m thick. The section below is composed mostly of epiclastic volcanic breccias and tuffs, while the section above is composed of andesitic lava flows, ash-flow tuffs, and epiclastic breccias.

0.3 Ma (Hiza, 1999). An interpretation of Hiza's maximum age estimate suggests that volcanism at Sepulcher Mountain commenced by 53 Ma.

Three generalized stratigraphic sections for the volcanic sequence at Sepulcher Mountain are presented in Figure 8. The locations of these sections are identified in Figure 3. The volcanic sequence at Stephens Creek (A-A') and the north ridge (B-B') of Sepulcher Mountain grade upward from predominately alluvial facies epiclastic breccias to vent facies lava flows and dikes. The section at the north spur (C-C') of Sepulcher Mountain notably lacks the lower epiclastic breccias and the entire exposed section is compositionally similar to the upper sections at Stephens Creek and at the north ridge. This feature likely results from stratigraphic offset along the normal fault discussed above.

The stratigraphic section at the north ridge is dominated by andesites with subordinate basaltic andesites and dacites, whereas rocks at the north spur are more silicic with dacites dominating the stratigraphic section (Figure 8). However, this compositional feature may be exaggerated due to a more restricted data set from this locality. A weakly defined compositional trend is apparent at the north ridge section where rocks exhibit increasingly silicic and potassic compositions with higher stratigraphic position. Spatial variations are more pronounced than stratigraphic variations in bulk chemistry in the Sepulcher Mountain volcanic sequence.

Texturally and compositionally, dikes and lava flows at Sepulcher Mountain are very similar to each other. They are both typically fine-to medium-grained, porphyritic, orthopyroxene + clinopyroxene andesites and biotite + amphibole dacites. Dikes are more abundant than lava flows on the east side of Sepulcher Mountain although the

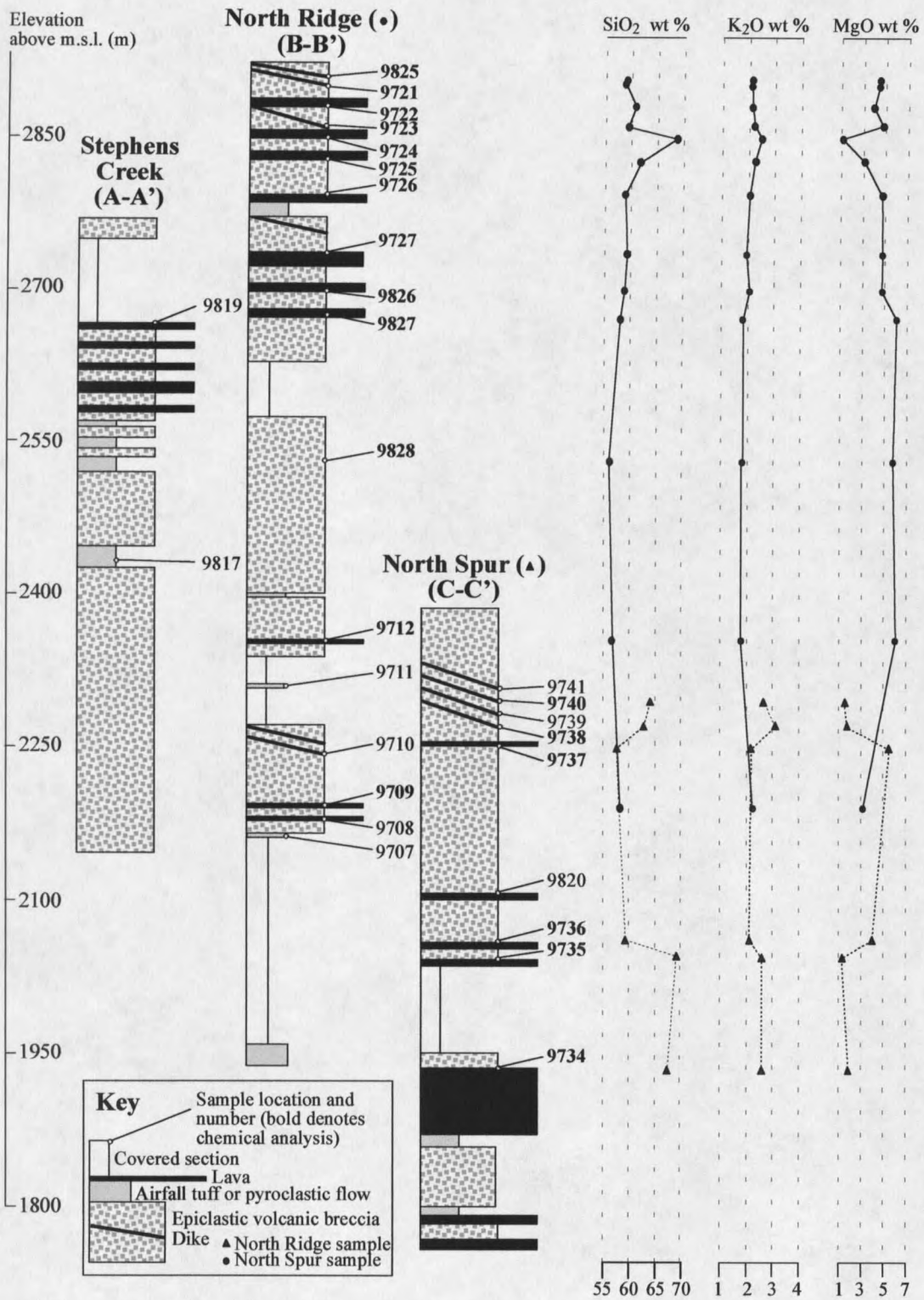


Figure 8. Generalized stratigraphic sections for volcanic sequences at Sepulcher Mountain. Major element oxide concentrations for analyzed rocks (bold labels) are plotted on the right. Circles represent data for rocks from the North Ridge, triangles represent data for rocks from the North Spur. Locations of stratigraphic sections are shown in Figure 3.

previously mapped extent of the prominent dike swarm (U.S. Geological Survey, 1972; Figure 3) was not recognized.

Geological Relationships Between Intrusive and Volcanic Rocks

Intrusive and volcanic rocks from Electric Peak and Sepulcher Mountain exist in close proximity (<5 km) to each other and exhibit broadly similar compositional ranges. The volcanic sequence at Sepulcher Mountain is separated from the Electric Peak stock by a normal fault that exhibits more than 600 m of stratigraphic offset. Together, features described above suggest that intrusive and extrusive rocks are related, and that the Electric Peak stock represents a shallow intrusion associated with the volcanic sequence preserved at Sepulcher Mountain. These interpretations are, however, not easily reconcilable with the age determinations of Hiza (1999).

Crosscutting field relationships indicate that the Electric Peak stock is younger than 50.0 Ma and the principle of superposition indicates that the volcanic Sequence at Sepulcher Mountain is younger than 53.4 Ma. Similar, intermediate-composition, moderate volume magmatism at a single eruptive center in the Andes spans approximately 1 m.y. (Signer et al., 1997). In this respect, more than 3 m.y. of magmatism at Electric Peak and Sepulcher Mountain is unlikely to be derived from a single, moderate volume magmatic system. Hiza's age determination for the Sepulcher block and ash-flow tuff is, however, an interpretation of a disturbed Ar spectrum. Moreover, it represents only a maximum age for the inception of volcanism at Sepulcher Mountain. The majority of primary volcanic rocks present at Sepulcher Mountain are

stratigraphically separated from this block and ash-flow tuff by ~700 m of epiclastic breccias and covered sections (Section B-B', Figure 8). One or more unconformities representing depositional hiatuses may be present, but difficult to identify in these rocks. It is therefore likely that magmatism at Electric Peak and Sepulcher Mountain are roughly contemporaneous. Further geochronologic study would be required in order to better document the timing of this magmatism. In light of these field relationships and existing geochronologic data, intrusive rocks at Electric Peak and volcanic rocks at Sepulcher Mountain are interpreted as comagmatic, derived from similar magmatic systems. The intrusive rocks at Electric Peak are not, however, interpreted to represent subvolcanic magma chambers or crustal conduits for the volcanic rocks at Sepulcher Mountain. Instead, they simply represent small-volume, discrete magmatic injections into shallow crustal levels. Discussion of the petrography, chemistry, and petrogenesis of these rocks will further clarify the nature of this relationship.

CHAPTER 3

ANALYTICAL METHODS

Rock samples of one to two kg were collected from outcrops distributed across the entire field area. Sample locations are shown on Figure 3 and UTM coordinates are listed in Appendix A. The investigated suite consists of 41 volcanic and 17 intrusive samples. Volcanic samples were collected from 26 lava flows, nine dikes, three clasts from lava flow autobreccias, and two magmatic inclusions. Intrusive samples were collected from five different intrusive phases of the Electric Peak stock, three dikes, and two cumulate inclusions.

Major and trace element, isotopic, and modal analyses were conducted on select, fresh samples. Major element oxide compositions and concentrations of V, Cr, Ni, Zn, Rb, Sr, Y, Zr, Nb, Ba, Pb, and Th were determined by standard X-ray fluorescence (XRF) spectrometry. A minimum of 100 g of each sample (chipped at the outcrop) was shipped to Washington State University, Pullman, for sample preparation and analysis using an automated Rigaku 3370 XRF Spectrometer by the GeoAnalytical Laboratory following the protocol described by Johnson and others (1999). The oxidation state of iron was ignored during analyses and subsequently calculated and reported in this study as ferric (Fe_2O_3) based on the assumption that ferrous iron is oxidized during ignition at temperatures of $\sim 1000^\circ\text{C}$ prior to XRF analysis. Loss on ignition (LOI) was not determined.

Instrumental neutron activation analyses (INAA) were performed at the Oregon State University Triga Reactor facility following the procedure outlined by Laul (1979). Prior to irradiation at least 50 g of sample were powdered in an alumina shatterbox to avoid contamination by Co and W. Estimated precision on the INAA analyses is better than 3% (1σ S.D.) for Sc and La; 5% for Co, Cs, Hf, Ta, Th, Sm, Eu, Tb, Yb, and Lu; and 7-12% for U, Ce, and Nd. Trace element concentrations for two samples were determined through inductively coupled plasma mass spectroscopy (ICP-MS) at the GeoAnalytical Laboratory at Washington State University, Pullman. These two samples were analyzed using a Siex-Elan model 250 ICP-MS following the protocol described by Lichte et al. (1987).

Whole rock powders from select, fresh samples were shipped to the W.M. Keck Foundation National Center for Isotope Geochemistry, University of California, Los Angeles. Sr and Nd isotopic compositions of Sr and Nd were determined by thermal ionization mass spectrometry (TIMS), following the procedure described by Feeley and Davidson (1994). Prior to isotopic determinations, Sr and Nd separations were performed using the methods described by Halliday et al. (1989) and Richard et al. (1976). Precision on Sr and Nd isotopic determinations (2σ S.D.) is better than ± 0.000013 and ± 0.00009 respectively.

Chemical analyses of mineral phases from representative samples spanning the compositional range were performed at Oregon State University Electron Microprobe Laboratory and at the University of Lausanne, Switzerland using Cameca SX-50 electron microprobes. Both synthetic and natural phases close in composition to the unknowns were used as standards. Data were corrected for matrix interference using the ZAF

method; a 15 kV accelerating voltage along with a 10 nA beam current were used for plagioclase analyses. A 20 nA current was used for analyses of all other phases.

Modal data were determined by point counting following the method described by Chayes (1956) and Hutchison (1974). Between 1200-1500 points per thin section were counted for the extrusive samples, with phenocrysts defined as ≥ 0.3 mm in the longest dimension. Approximately 1000 points were counted per thin section for the intrusive samples, with phenocrysts defined as ≥ 0.1 mm in the longest dimension. An attempt was made to identify and count only primary mineral phases if secondary alteration products including chlorite, iddingsite, and sericite were recognized. Vesicles and secondary, void-filling minerals such as silica and calcite were initially included in the modal analyses although their proportions were subsequently subtracted from the total number of counted points in order to acquire dense, unaltered rock equivalents.

CHAPTER 4

PETROGRAPHY, MINERAL COMPOSITIONS, AND
MAGMATIC INTENSIVE PARAMETERS

Modal analyses of thin-sections and microprobe studies of common silicate and Fe-Ti oxide minerals were conducted for the purpose of characterizing the mineralogy of EPSM rocks, for estimating magmatic intensive parameters, and for use in quantitative petrologic modeling. Detailed petrographic descriptions of individual rocks are given in Appendix A.

PetrographySepulcher Mountain and Peripheral Volcanic Vents

Dikes and lava flows from Sepulcher Mountain and peripheral volcanic vents are typically hypocrystalline, fine-to medium-grained, porphyritic to glomeroporphyritic, seriate, and often sub-trachytic. Total phenocryst contents range from 8 to 43% (by volume) with the total increasing with increasing SiO₂ contents until 66 wt% SiO₂. Phenocryst contents decrease with increasing SiO₂ contents at compositions >66 wt% SiO₂.

Changes in phenocryst mode are fairly regular with respect to bulk composition (Figure 9). For example, modal proportions of olivine and clinopyroxene decrease with increasing SiO₂ and are essentially absent in rocks with >60 and >65 wt% SiO₂ respectively; whereas amphibole and biotite are essentially present only in rocks with

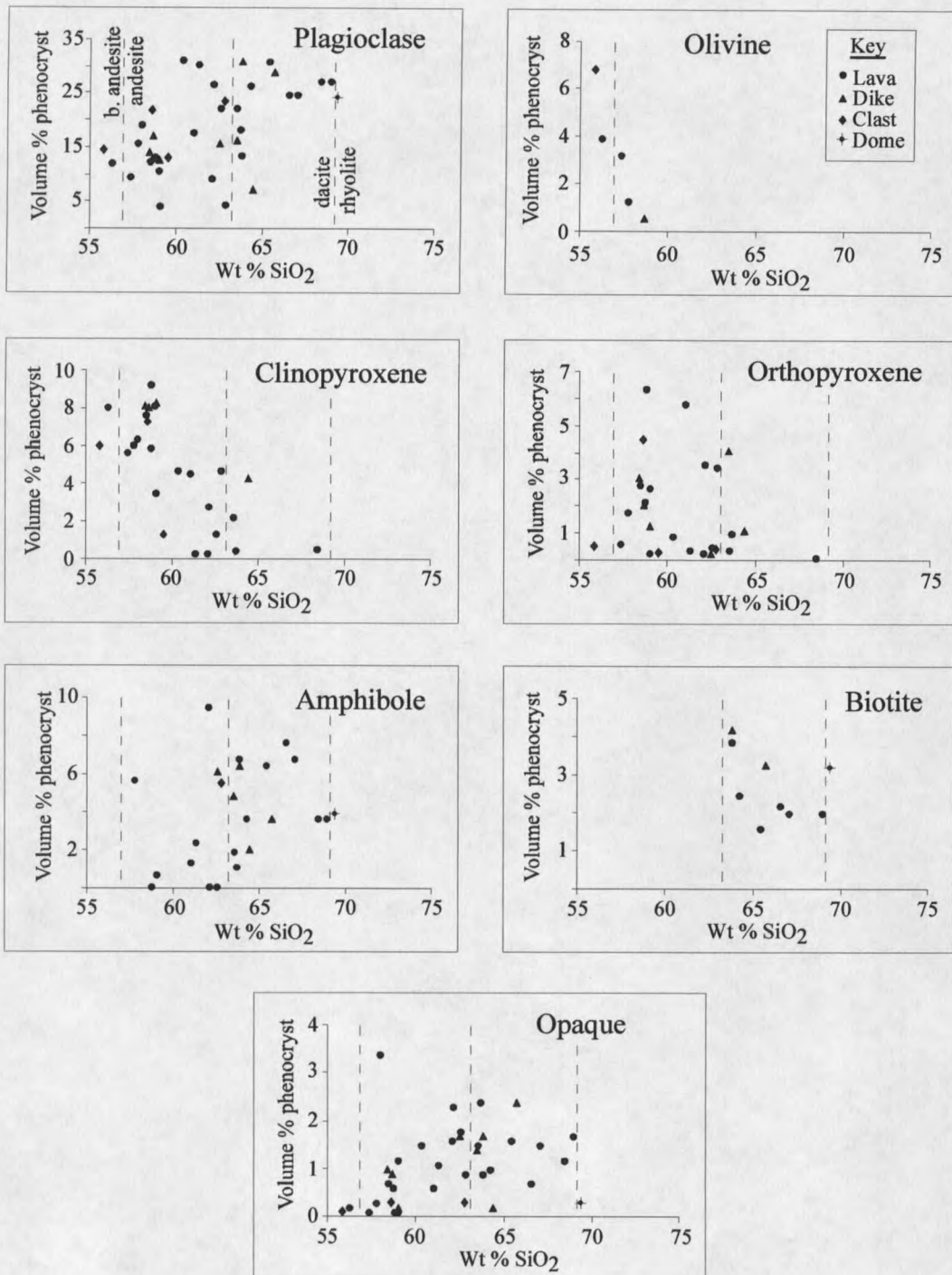


Figure 9. Variation of modal abundances of phenocryst phases in extrusive rocks from Sepulcher Mountain versus whole rock SiO₂ wt%.

>60 and >65 wt% SiO₂, respectively. Specifically, basaltic-andesitic rocks contain plagioclase > clinopyroxene > olivine > orthopyroxene; andesitic rocks contain plagioclase > clinopyroxene > orthopyroxene ± amphibole ± olivine; dacites contain plagioclase > amphibole > biotite ± clinopyroxene ± orthopyroxene; and rhyodacitic rocks contain plagioclase > amphibole > biotite > quartz.

Groundmass in rocks from dikes and lava flows at Sepulcher Mountain consists of microphenocrysts and partially-to-completely devitrified glass. Plagioclase microlites and Fe-Ti oxide microphenocrysts are present in all rocks. Modal proportions of Fe-Ti oxide phases roughly increase with increasing SiO₂ contents until about 66 wt% SiO₂. Glomerocrysts are common and typically contain solitary orthopyroxene, clinopyroxene > orthopyroxene ± Fe-Ti oxides, or clinopyroxene > orthopyroxene > plagioclase ± Fe-Ti oxides. Apatite is a common accessory mineral and is often included in plagioclase. Although rare, disequilibrium textures in amphibole, pyroxene, and plagioclase phenocrysts are present in some rocks and were identified by the presence of magmatic reaction textures including coronae, mantling, and dissolution textures.

Magmatic inclusions (c.f. Bacon, 1986) are only recognized within the Rainbow Lakes rhyodacite dome (Figure 3). These inclusions include fine- to medium-grained, holocrystalline amphibole-trachyandesite and undercooled, fine-grained amphibole-andesite. The holocrystalline inclusions are mineralogically similar to the hornblende gabbro inclusions contained within the granodiorite phase of the Electric Peak stock.

Electric Peak Stock

Rocks from the Electric Peak stock exhibit significant textural diversity. Dikes are typically hypocrystalline, fine- to medium-grained, and porphyritic; they are texturally very similar to dikes from Sepulcher Mountain. Holocrystalline intrusive phases of the Electric Peak stock are fine- to medium-grained, seriate, and inequigranular (Figure 10). In light of these textural features, these rocks are herein referred to as micro-porphyrries. Although these rocks appear medium- to coarse-grained in hand sample, petrographic inspection reveals that the exaggerated coarse-grained appearance is the result of mafic and felsic mineral glomerocrysts (i.e. numerous plagioclase laths or amphibole crystals lumped together).

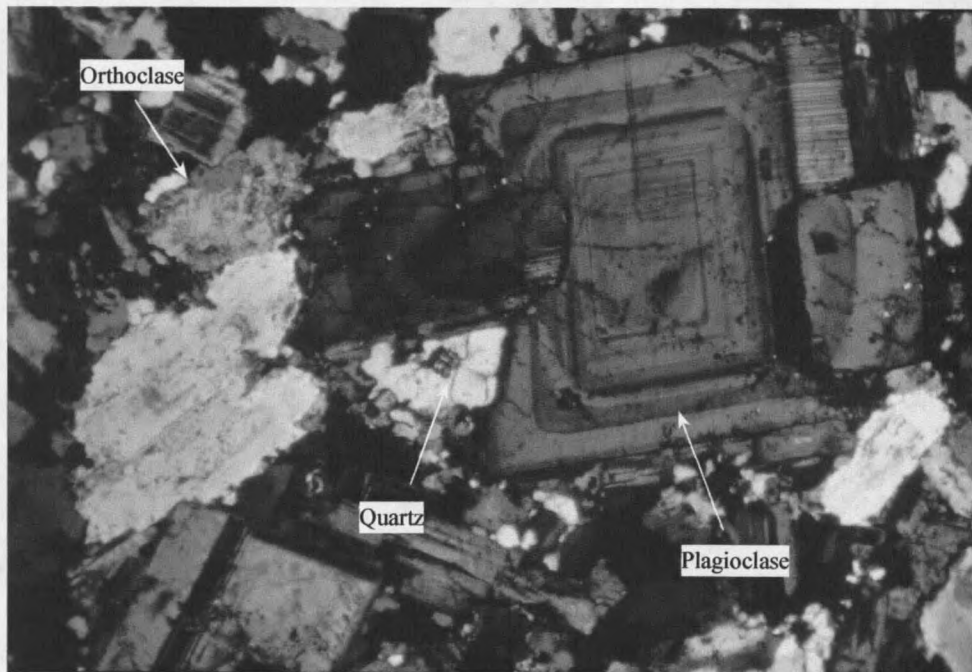


Figure 10. Medium-grained, holocrystalline, inequigranular texture representative of micro-porphyrries from the Electric Peak stock (EP9718, crossed-polars, 45X magnification, field of view = 2.8 mm).

Changes in mode for dikes and micro-porphyrries from Electric Peak are not as apparent with respect to bulk composition as they are for lavas and dikes from Sepulcher Mountain (Figure 11). Dioritic rocks (57-63 wt% SiO₂) contain plagioclase >> quartz > amphibole + biotite ± orthoclase. Granodioritic rocks (63-69 wt% SiO₂) contain plagioclase >> quartz > orthoclase > biotite + amphibole. Granitic rocks (69-73 wt% SiO₂) contain plagioclase >> orthoclase + quartz > biotite > amphibole. Pyroxene is only present in one sample from the quartz diorite phase of the stock. Modal proportions of plagioclase, amphibole, and biotite decrease with increasing SiO₂. Modal proportions of orthoclase and, to a lesser extent, quartz increase with increasing SiO₂. A marked inflection in modal trends is present at ~69 wt% SiO₂ for all mineral phases except quartz. Opaque minerals are present in all rocks from Electric Peak and include Fe-Ti oxides and Fe-Cu sulfides. Apatite, zircon, allanite, zoisite, and sphene are very rare accessory phases.

Inclusions are abundant in the granodiorite phase of the Electric Peak stock. These include sedimentary and metamorphic xenoliths, as well as hornblende gabbro magmatic inclusions. Sedimentary xenoliths include fragments of country rock (Cody Shale and Frontier Sandstone) that are abundant near intrusive contacts. Minor evidence for thermal or chemical interaction between xenoliths and intrusive host rock indicates incorporation at near solidus temperatures. Metamorphic xenoliths include gneissic granitoids and amphibolites, and are lithologically similar to Archean metamorphic rocks from the Beartooth Mountains. Hornblende gabbro inclusions (Figure 12) are abundant at the base of the granodiorite phase of the stock. They are holocrystalline, medium- to coarse-grained, inequigranular, and contain amphibole >> plagioclase >>> quartz + Fe-Ti

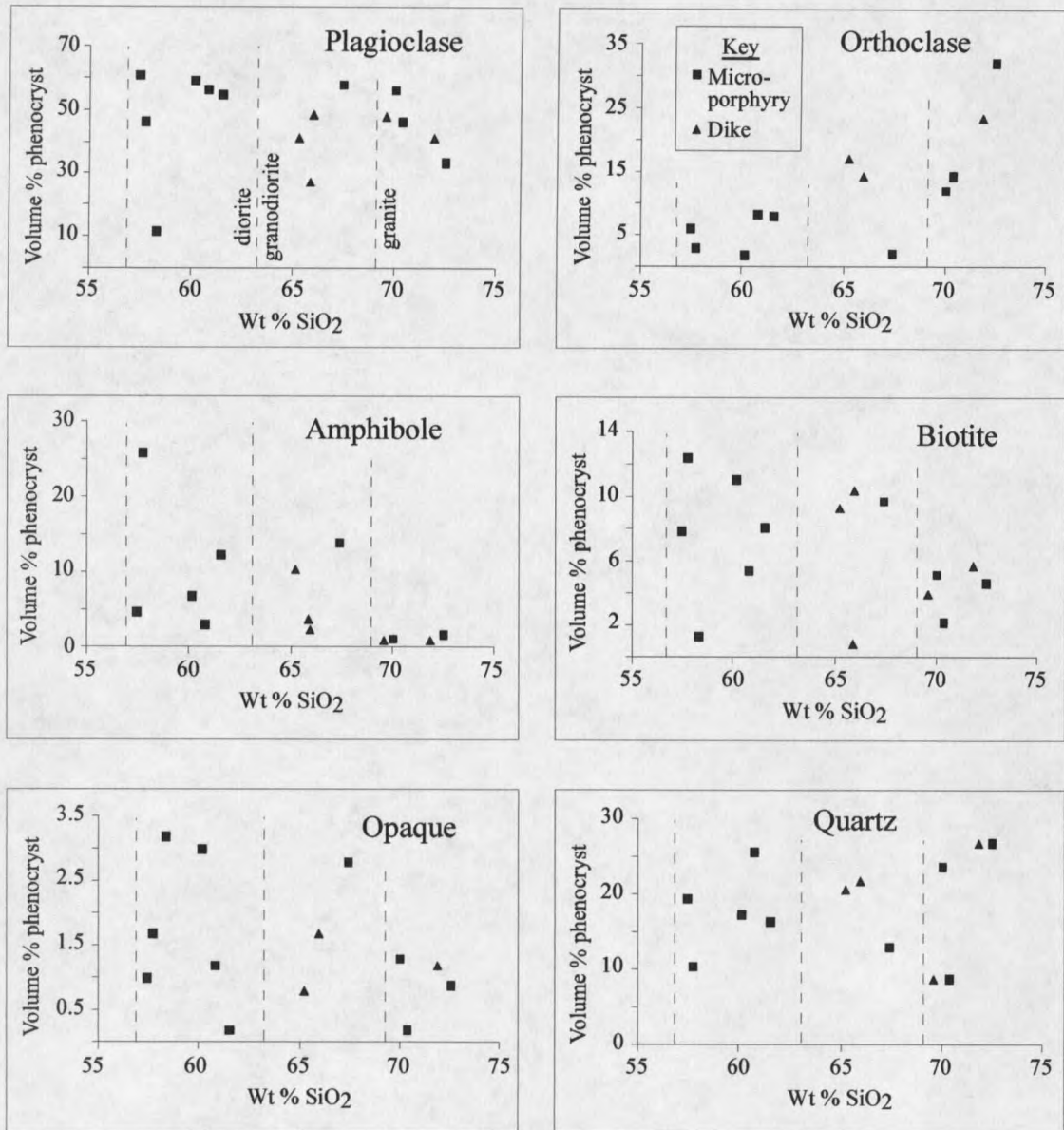


Figure 11. Variation of modal abundances of mineral phases in intrusive rocks from Electric Peak versus whole rock SiO₂.

oxides \pm biotite. Amphibole in these inclusions is estructural with medium integrity and is reacting to biotite + Fe-Ti oxides. Plagioclase is locally poikilitic around amphibole and exhibits both step and regular progressive zoning. Quartz appears to be interstitial and crystallized after amphibole and plagioclase.

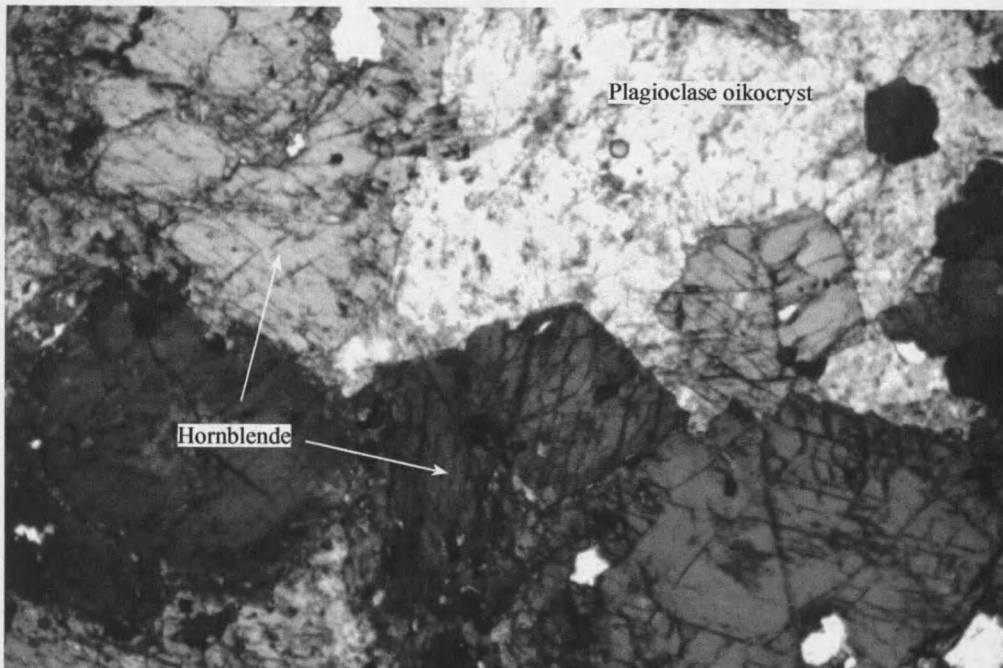


Figure 12 . Coarse-grained, holocrystalline hornblende gabbro inclusion from the base of the granodiorite phase (EP9714) of the Electric Peak stock (EP9847, plane light, 25X magnification, field of view = 2.8 mm).

Mineral Compositions

The compositions of eight mineral phases (clinopyroxene, orthopyroxene, plagioclase feldspar, orthoclase feldspar, amphibole, biotite, ilmenite, and magnetite) in eight rocks (six extrusive and two intrusive rocks) from the EPSM complex that collectively span the compositional range of the suite were determined by electron

microprobe analysis. Major element compositions of mineral phases in EPSM rocks are reported in Appendices B-F. The representative chemical compositions and end-member proportions presented for these minerals in Tables 1-6 were calculated using the mean of compositional data acquired for a specific mineral phase within one rock.

Plagioclase Feldspar

Plagioclase is the most abundant mineral in rocks from the EPSM complex, with the exception of a few andesitic rocks in which clinopyroxene and amphibole are slightly more abundant. Plagioclase grains exhibit a wide range of textures. It is predominately the largest mineral phase in both extrusive and intrusive rocks, although it is occasionally subordinate to amphibole in size. Crystals are typically sub-to-euhedral, compositionally zoned, and frequently exhibit textures caused by alternating periods of crystal growth and dissolution, perhaps induced by thermal or chemical disequilibrium (Figure 13). Plagioclase laths often exhibit mantling of resorbed crystal boundaries. Crystal cores occasionally exhibit a spongy, cellular texture. Although plagioclase is usually fresh in volcanic rocks, sericitized cores are common in intrusive samples. When present, directional fabrics such as trachytic texture, are most strongly developed among plagioclase grains.

Representative plagioclase core and rim compositions are presented in Table 1 and feldspar solid solution ternary end-member proportions are illustrated in Figure 14. Anorthite proportions range from An₆₁ to An₅₃ in low-silica (~58 wt%) andesitic rocks, from An₆₄ to An₂₇ in low-silica (~63 wt%) dacites, and from An₄₉ to An₃₁ in rhyodacites (~69 wt% SiO₂). Low-silica dacites exhibit the widest range of anorthite proportions, but

this may reflect the larger number of analyses for this rock type. Feldspars were only analyzed in two intermediate-composition intrusive rocks and anorthite proportions in these rocks range from An₄₉ to An₁₂, notably more sodic than plagioclase in extrusive samples. This may reflect lower crystallization temperatures for the intrusive rocks.

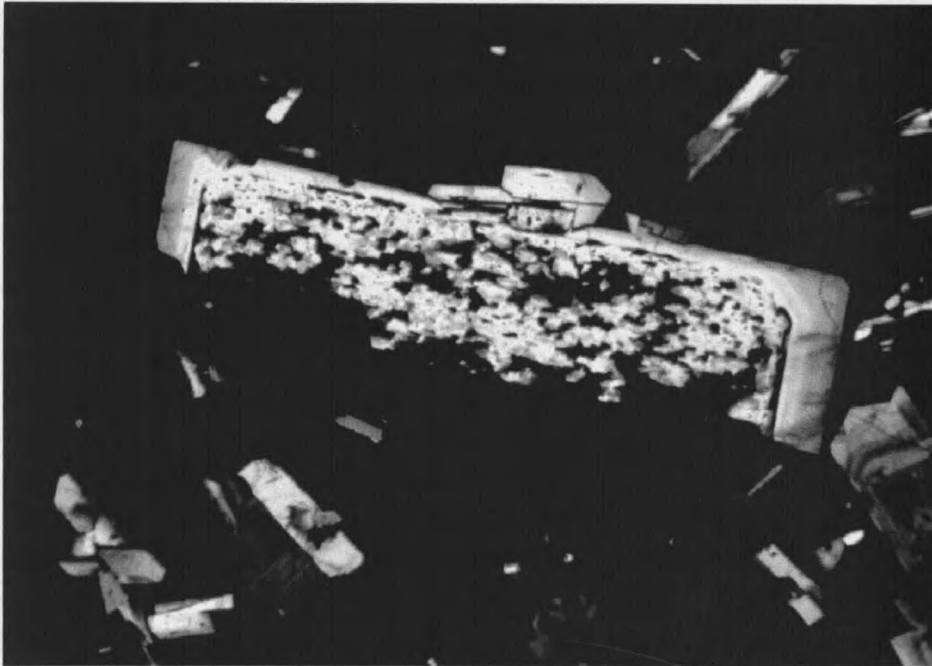


Figure 13. Plagioclase phenocryst exhibiting a euhedral rim mantling a spongy cellular core (SM9713, crossed-polars, 100X magnification, field of view = 1.05 mm).

The majority of plagioclase grains (90%) in andesitic rocks are reversely zoned (Figure 14a). However, the maximum extent of reverse zoning in plagioclase grains in andesitic rocks is 10 mol% An, and over half of the grains analyzed in these rocks exhibit reverse zoning of less than 7 mol% An. Low-silica dacites contain roughly equal proportions of normally and reversely zoned plagioclase (Figure 14b). The maximum

Table 1. Representative feldspar compositions.

Sample	(SiO ₂)	Remark	n	SiO ₂	Al ₂ O ₃	FeO*	CaO	Na ₂ O	K ₂ O	An	Ab	Or	An range
SM9721	58.38	cores	7	52.28 (0.32)	28.97 (0.19)	0.63 (0.02)	11.77 (0.21)	4.59 (0.12)	0.30 (0.01)	57.6	40.64	1.75	53 to 61
SM9721	58.38	rims	6	51.75 (0.12)	29.73 (0.22)	0.72 (0.08)	12.84 (0.15)	3.95 (0.08)	0.23 (0.00)	63.37	35.27	1.35	61 to 65
SM9825	58.67	cores	5	52.85 (0.42)	29.60 (0.29)	0.62 (0.03)	12.14 (0.31)	4.26 (0.15)	0.28 (0.02)	60.16	38.19	1.65	57 to 64
SM9825	58.67	rims	3	51.88 (0.32)	30.34 (0.38)	0.71 (0.04)	12.77 (0.34)	4.03 (0.14)	0.24 (0.02)	62.76	35.84	1.4	60 to 64
SM9814	63.53	cores	14	56.69 (0.61)	27.01 (0.42)	0.27 (0.01)	8.85 (0.47)	6.10 (0.22)	0.36 (0.03)	43.56	54.33	2.11	27 to 55
SM9814	63.53	rims	18	56.84 (0.24)	26.73 (0.16)	0.32 (0.01)	8.49 (0.21)	6.22 (0.12)	0.38 (0.01)	42.04	55.72	2.24	33 to 51
SM9740	63.84	cores	11	55.37 (0.45)	27.75 (0.36)	0.21 (0.02)	9.78 (0.40)	5.56 (0.19)	0.29 (0.03)	48.45	49.84	1.71	41 to 64
SM9740	63.84	rims	10	57.08 (0.23)	26.76 (0.22)	0.22 (0.01)	8.61 (0.20)	6.13 (0.09)	0.35 (0.01)	42.8	55.13	2.07	38 to 48
SM9724	68.43	cores	9	56.97 (0.44)	27.07 (0.33)	0.32 (0.03)	8.74 (0.33)	6.21 (0.15)	0.32 (0.03)	42.93	55.19	1.87	35 to 49
SM9724	68.43	rims	6	58.27 (0.87)	25.82 (0.51)	0.29 (0.02)	7.51 (0.59)	6.76 (0.30)	0.45 (0.04)	37.04	60.32	2.64	31 to 46
SM9735	68.95	cores	11	56.33 (0.33)	26.47 (0.26)	0.32 (0.03)	8.23 (0.28)	6.49 (0.14)	0.38 (0.02)	40.29	57.49	2.22	31 to 48
SM9735	68.95	rims	9	57.48 (0.29)	25.63 (0.07)	0.25 (0.01)	7.29 (0.08)	7.03 (0.05)	0.40 (0.01)	35.59	62.09	2.32	34 to 37
EP9714	61.59	cores	3	57.31 (1.06)	27.06 (0.51)	0.23 (0.05)	8.79 (0.65)	6.22 (0.34)	0.39 (0.06)	42.86	54.88	2.26	37 to 49
EP9714	61.59	rims	3	64.33 (1.26)	22.79 (0.73)	0.16 (0.01)	3.75 (0.86)	9.0 (0.52)	0.59 (0.03)	18.08	78.53	3.33	12 to 26
EP9845	65.97	cores	4	57.67 (1.62)	26.51 (1.14)	0.23 (0.05)	8.17 (1.26)	6.58 (0.72)	0.37 (0.05)	39.02	8.03	2.15	22 to 48
EP9714	61.59	cores	5	64.69 (0.15)	18.45 (0.07)	0.10 (0.03)	0.01 (0.01)	1.05 (0.33)	15.24 (0.44)	0.05	9.47	90.48	-
EP9845	65.97	core	1	63.82	19.28	0.07	0.19	2.92	12.01	0.96	26.73	72.31	-

Note: (SiO₂) = whole rock silica content; n = number of analyses from which mean and standard deviation were calculated; An, Ab, and Or are calculated proportions of Anorthite, Albite, and Orthoclase respectively; An range = range of anorthite proportions observed in all analyses from which representative compositions were calculated; values in parentheses represent one standard deviation of the mean. All Fe as FeO*.

extent of normal zoning in plagioclase grains in low-silica dacitic rocks is 29 mol% An, and over half of these grains exhibit normal zoning of less than 7 mol% An. Alternately, the maximum extent of reverse zoning of plagioclase in low-silica dacitic rocks is 15 mol% An, and over half of these grains exhibit reverse zoning of less than 5 mol% An. Plagioclase grains in rhyodacitic samples are almost entirely (93%) normally zoned (Figure 14c). The maximum extent of normal zoning in plagioclase grains in rhyodacitic rocks is 15 mol% An, and over half of these grains exhibit normal zoning of less than 7 mol% An.

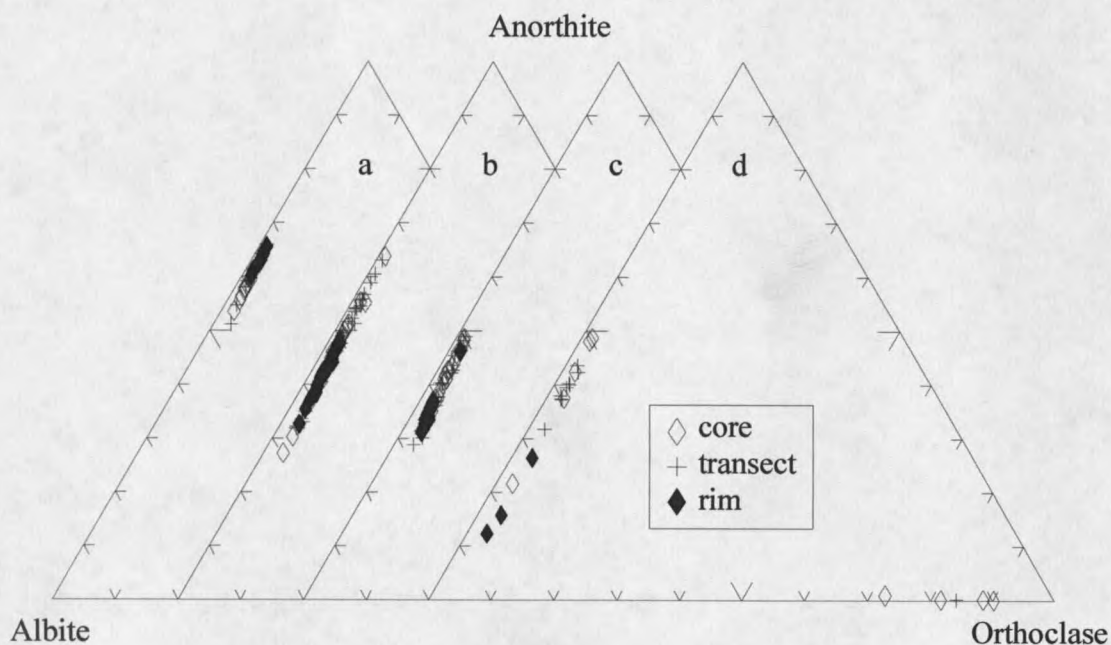


Figure 14. Ternary projections of feldspar compositions of extrusive rocks from Sepulcher Mountain and intrusive rocks from Electric Peak grouped by whole rock compositional series. Compositional series: (a) low-silica (58%) andesites, (b) low-silica (63%) dacites, (c) rhyodacites (69%), and (d) intermediate (65% SiO₂) intrusive rocks. Each point represents a single analysis.

Orthoclase Feldspar

Orthoclase is only present in holocrystalline rocks from Electric Peak. It is commonly fine-grained, uniquely associated with quartz, and interstitial to other mineral phases. Petrographically, orthoclase grains do not exhibit evidence for unmixing into Na- and K-rich phases. Due to its fine-grained, interstitial character orthoclase feldspar is extremely difficult to identify in unstained thin sections from these rocks. Therefore, modal abundances plotted in Figure 11 for unstained sections (7 of 15) are semi-qualitative.

Representative orthoclase compositions are presented in Table 1 and feldspar solid solution ternary end-member proportions are illustrated in Figure 14d. Orthoclase grains contain limited Na and almost no Ca. Orthoclase end-member proportions range from Or₉₂ – Or₇₂ in granodioritic rocks and Ba end-member Celsian components are less than 1 mol%.

Olivine

Olivine is present only in five lavas and dikes from Sepulcher Mountain and is restricted to those with <59 wt% SiO₂. As olivine is almost always completely altered to iddingsite and serpentine, no attempt was made to characterize olivine compositions optically or chemically.

Clinopyroxene

Clinopyroxene is the most dominant mafic mineral phase in basaltic-andesitic and andesitic lavas and dikes from Sepulcher Mountain. It is only present in one rock (a dike) from Electric Peak. Clinopyroxene occurs in volcanic rocks as isolated, euhedral to subhedral phenocrysts, and is often contained in glomerocrysts where it is typically associated with orthopyroxene. It is also present as a microphenocryst and groundmass phase.

Representative compositions of clinopyroxene are given in Table 2 and ternary end-member proportions are illustrated in Figure 15. Clinopyroxene in andesitic rocks ranges in composition from $Wo_{42}En_{44}Fs_{08}$ to $Wo_{43}En_{49}Fs_{14}$ (Table 2). Following the nomenclature of Morimoto et al. (1988), clinopyroxene compositions are predominately classified as augite, although a few rocks contain crystals with endiopside cores. Most clinopyroxene cores exhibit normal compositional zoning with rims becoming more Fe-rich than cores (Figure 15). Cores commonly exhibit more compositional variability than rims, which are dominantly $Wo_{43}En_{47}Fs_{10}$.

Orthopyroxene

Orthopyroxene is present in andesitic and a few low-silica dacitic lavas and dikes from Sepulcher Mountain and is also present in one quartz diorite dike from Electric Peak. It is almost always associated with clinopyroxene, although it is less abundant. Orthopyroxene is present both in glomerocrysts with clinopyroxene and opaque minerals and as solitary phenocrysts. It is almost always euhedral.

Table 2. Representative clinopyroxene compositions.

Sample	Remarks	(SiO ₂)	n	SiO ₂	TiO ₂	Al ₂ O ₃	Fe ₂ O ₃ *	FeO*	MnO	MgO	CaO	Wo*	En*	Fs*
SM9721	Cores	58.38	11	51.74 (0.18)	0.52 (0.39)	2.56 (0.23)	2.74 (0.10)	6.37 (0.42)	0.25 (0.01)	15.93 (0.26)	20.30 (0.17)	40-43	41-48	10-18
SM9721	Rims	58.38	3	52.00 (0.39)	0.50 (0.04)	2.11 (0.28)	2.83 (0.37)	6.36 (0.41)	0.26 (0.04)	16.13 (0.12)	20.48 (0.21)	40-41	44-45	14-15
SM9825	Cores	58.67	9	52.33 (0.26)	0.30 (0.05)	2.08 (0.16)	2.94 (0.23)	4.13 (0.37)	0.17 (0.01)	17.13 (0.29)	20.64 (0.14)	40-43	44-50	5-9
SM9825	Rims	58.67	1	51.14	0.51	2.08	3.46	5.52	0.22	15.72	20.55	-	-	-

Note: (SiO₂) = whole rock silica content; n = number of analyses from which mean and standard deviation were calculated;

Fe₂O₃*, FeO* = Fe⁺³ and Fe⁺² determined by charge balance; values in parentheses represent one standard deviation

of the mean; Wo*, En*, Fs* are the range of observed ternary endmember proportions observed in all analyzed grains.

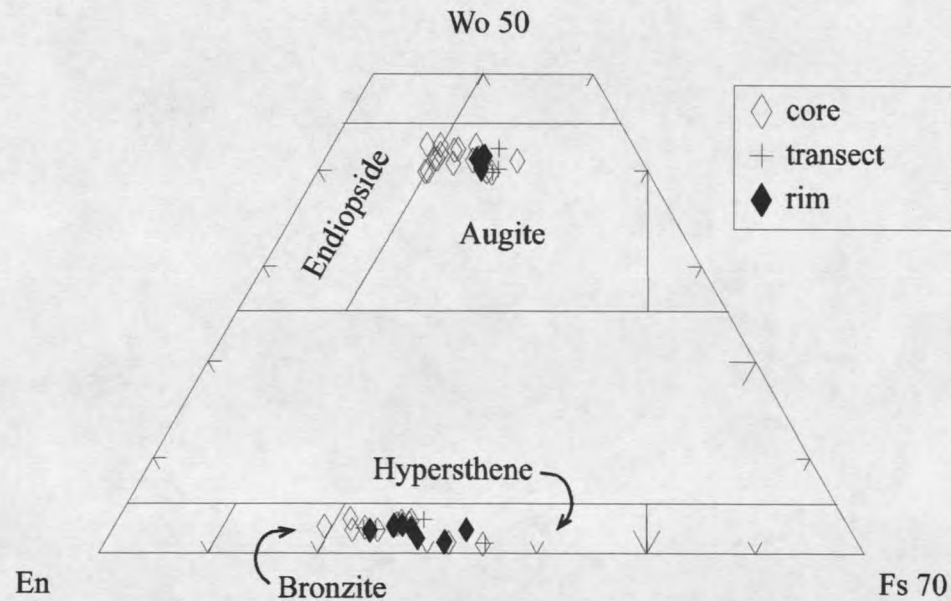


Figure 15. Ternary projection and classification of pyroxenes in extrusive rocks from Sepulcher Mountain (after Morimoto, et al., 1988). Each point represents one analysis.

Representative orthopyroxene compositions are presented in Table 3 and end-member proportions are illustrated in Figure 15. Compositions in andesitic rocks range from $Wo_{01}En_{68}Fs_{20}$ to $Wo_{03}En_{77}Fs_{31}$. Orthopyroxene are classified as hypersthene following the nomenclature of Morimoto and others (1988). Although core compositions are diverse, rim compositions are less variable and are predominately $Wo_{03}En_{72}Fs_{25}$.

Amphibole

Apart from plagioclase, amphibole is the most salient mineral phase in rocks from the EPSM complex. It is present in all lavas and dikes with >58 wt% SiO_2 and in all but two intrusive rocks from Electric Peak. Amphibole exhibits distinctive textures in both volcanic and intrusive rocks. In extrusive rocks it occurs as small (< 1.0 mm) euhedral crystals, often with oxidized rims, although it also occurs as larger (0.5 - 1.75 mm) predominately eustructural crystals with medium structural integrity. In these grains both the margins and the interior of these crystals exhibit a boxy cellular texture bounded by crystal faces. Amphibole in intrusive rocks typically has partially reacted to biotite and opaque minerals (Figure 16).

Amphibole phenocrysts in rocks from both the Electric Peak stock and Sepulcher Mountain lavas and dikes are calcic according to the nomenclature of the International Mineralogical Association Subcommittee (I.M.A.S.) on Amphiboles (Leake, 1978) because B-group cation occupancy ($Ca + Na$) is ≥ 1.34 and Na is ≤ 0.67 . Representative compositions are given in Table 4. Compositions were calculated on the basis of the 24-oxygen hydrous formula with H_2O calculated by difference and assuming that $Fe^{3+}/(Fe^{2+} + Fe^{3+})$ is fixed and = 0.27, a reasonable estimate for hornblende in calc-alkaline

Table 3. Representative orthopyroxene compositions.

Sample	Remarks	(SiO ₂)	n	SiO ₂	TiO ₂	Al ₂ O ₃	Fe ₂ O ₃ *	FeO*	MnO	MgO	CaO	Wo*	En*	Fs*
SM9721	Cores	58.38	16	54.30 (0.24)	0.25 (0.03)	1.13 (0.19)	2.28 (0.27)	14.90 (0.68)	0.39 (0.02)	26.81 (0.41)	1.62 (0.08)	2~3	69~76	22~28
SM9721	Rim	58.38	1	54.48	0.23	0.83	1.68	15.64	0.4	26.54	1.56	-	-	-
SM9814	Cores	63.53	3	52.81 (0.27)	0.14 (0.05)	1.58 (0.28)	2.22 (0.31)	19.14 (0.40)	0.74 (0.02)	23.92 (0.42)	0.51 (0.26)	1	64~68	31~35
SM9814	Rims	63.53	4	53.52 (0.53)	0.13 (0.01)	1.00 (0.22)	1.25 (0.46)	18.14 (0.39)	0.70 (0.02)	24.75 (0.49)	0.81 (0.16)	1~3	65~70	28~32
SM9825	Cores	58.67	8	53.32 (0.26)	0.18 (0.01)	1.92 (0.22)	3.14 (0.39)	12.38 (0.58)	0.30 (0.02)	27.56 (0.39)	1.52 (0.08)	2~4	71~78	19~26
SM9825	Rims	58.67	4	52.96 (0.43)	0.22 (0.02)	1.76 (0.23)	3.25 (0.56)	13.58 (0.78)	0.35 (0.01)	26.72 (0.41)	1.39 (0.06)	2~3	70~74	24~27

Note: (SiO₂) = whole rock silica content; n = number of analyses from which mean and standard deviation were calculated;

Fe₂O₃*, FeO* = Fe⁺³ and Fe⁺² determined by charge balance; values in parentheses represent one standard deviation

of the mean; Wo*, En*, Fs* refers to the range of observed ternary endmember proportions observed in all analyzed samples.

Table 4. Representative amphibole compositions from selected samples.

	SM9814	SM9740	SM9724	SM9735	EP9714
(SiO ₂)	63.53	63.84	68.43	68.95	61.59
n	13	9	11	8	5
SiO ₂	44.98 (0.51)	44.54 (0.38)	45.14 (0.39)	44.50 (0.76)	50.58 (0.35)
Al ₂ O ₃	10.46 (0.43)	10.54 (0.51)	10.52 (0.19)	10.47 (0.74)	5.36 (0.26)
FeO	8.95 (0.18)	9.07 (0.31)	8.44 (0.35)	9.54 (0.39)	8.15 (0.09)
Fe ₂ O ₃	3.68 (0.07)	3.73 (0.13)	3.47 (0.14)	3.92 (0.16)	3.35 (0.04)
MgO	14.70 (0.27)	14.55 (0.22)	15.09 (0.39)	14.21 (0.51)	16.62 (0.15)
CaO	10.86 (0.07)	10.93 (0.05)	10.89 (0.04)	10.85 (0.11)	11.09 (0.03)
Na ₂ O	1.87 (0.07)	1.95 (0.08)	2.00 (0.02)	1.99 (0.09)	1.28 (0.05)
K ₂ O	0.55 (0.03)	0.72 (0.04)	0.58 (0.07)	0.60 (0.05)	0.30 (0.02)
TiO ₂	1.69 (0.13)	1.84 (0.12)	1.73 (0.16)	1.90 (0.06)	0.87 (0.06)
Cr ₂ O ₃	0.04 (0.01)	0.02 (0.01)	0.08 (0.04)	0.02 (0.01)	0.03 (0.02)
MnO	0.21 (0.02)	0.19 (0.02)	0.15 (0.12)	0.18 (0.02)	0.36 (0.02)
H ₂ O*	1.82 (0.05)	1.74 (0.05)	1.71 (0.07)	1.64 (0.05)	1.92 (0.08)
Name	edenitic hornblende	edenitic hornblende	edenitic hornblende	edenitic hornblende	actinolitic hornblende

Note: (SiO₂) = whole rock silica content; n = number of analyses from which mean and standard deviation were calculated; Fe²⁺ and Fe³⁺ were calculated on the assumption that Fe³⁺/(Fe²⁺ + Fe³⁺) = 0.27; H₂O* = water calculated by difference; values in parentheses represent one standard deviation of the mean.

intrusions (Dodge et al., 1968; Hammarstrom, 1982 and 1984). An attempt was made to screen out compositions representing late-stage alteration rather than primary magmatic crystallization in the intrusive rocks by imposing Leake's (1971) proposed limit of $Si \leq 7.5$ for "igneous" amphiboles and by limiting the data set to analyses with $Ca \geq 1.6$. Furthermore, compositions of amphibole rims exhibiting petrographic evidence for subsolidus alteration were omitted. The range of amphibole compositions exhibited by the suite is illustrated in Figure 17, which is a plot of total Al (Al^T) versus tetrahedral Al (Al^{iv}). All compositions fall within Leake's (1971) proposed limits for Al^{vi} in igneous amphiboles. Figure 17 also illustrates the most pronounced compositional difference between amphiboles in the intrusive rocks and the extrusive rocks. Amphiboles contained within extrusive rocks consistently contain more total aluminum than those in intrusive rocks.

Amphibole classification is illustrated in Figure 18. Amphiboles range in composition from ferroan pargasite to actinolitic hornblende following the nomenclature recommended by the I.M.A.S. (Leake, 1978). Representative amphiboles from Electric Peak are predominately actinolitic-hornblende, while amphiboles from Sepulcher Mountain are predominately edenitic hornblende. In order to simplify this nomenclature, all amphiboles are considered "hornblendes" (Hawthorne, 1981) subsuming the appropriate names shown in Figure 18.

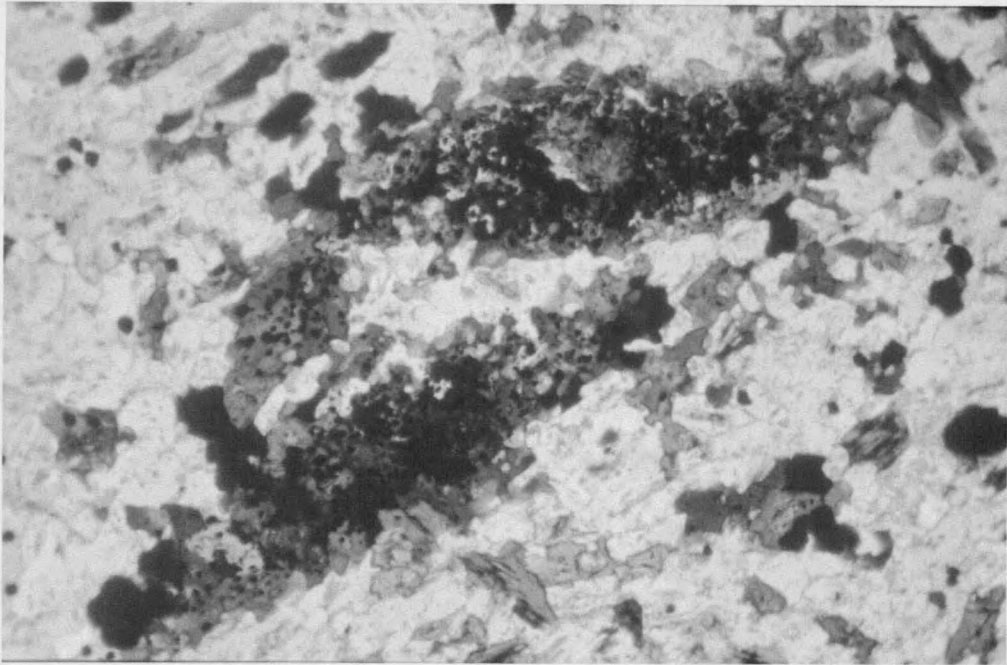


Figure 16. Eustructural amphibole with low structural integrity in a micro-porphyry from the Electric Peak stock. Amphibole has almost completely converted to biotite and Fe-Ti oxides (EP9715, plane light, 45X magnification, field of view = 2.8 mm).

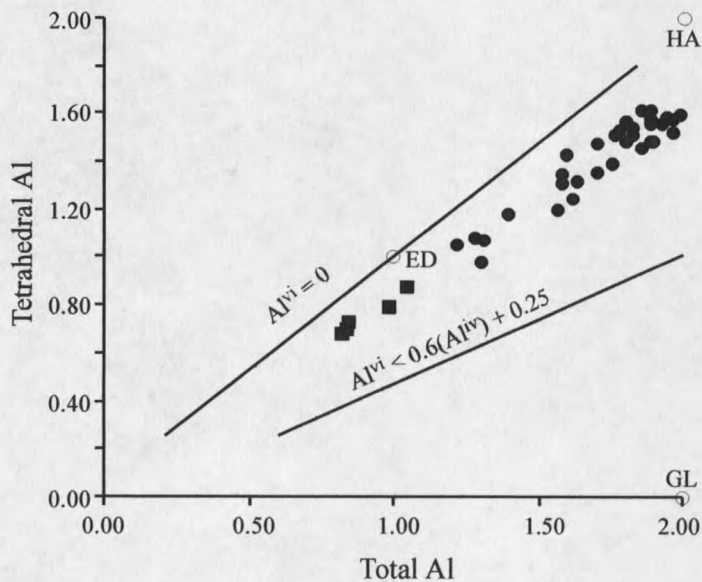


Figure 17. Plot of total Aluminum vs tetrahedral Aluminum in hornblende. Compositions from Electric Peak stock are shown as squares, compositions from Sepulcher Mountain lavas are shown as circles. The solid lines indicate the limiting condition for $Al^{VI} = 0$ and Leake's (1971) proposed limit for maximum possible Al^{VI} in calcic amphibole. Ideal endmember compositions are shown for edenite (ED), glaucophane (GL), and hastingsite (HA). All analyses were recalculated using a 24-oxygen hydrous formula unit; $Fe^{+3}/(Fe^{+2}+Fe^{+3}) = 0.27$, except for ED and GL where total $Fe=FeO$.

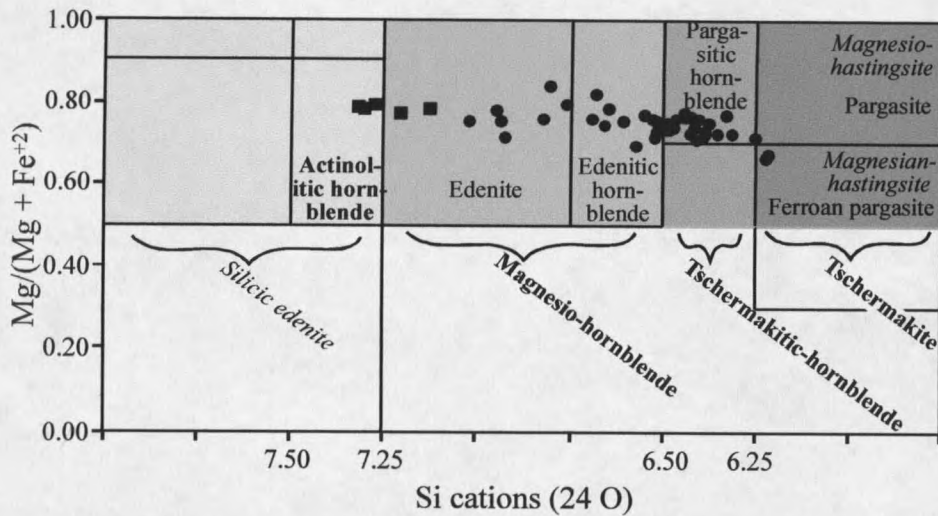


Figure 18. Classification of calcic-amphiboles (modified from Leake, 1978). Compositions from Electric Peak stock are shown as squares, compositions from Sepulcher Mountain lavas are shown as circles. Field names in diagonal orientation refer to shaded fields. Field names in bold type refer to nomenclature for A site $(Na + K) < 0.50$, $Ti < 0.50$, those in plain type refer to nomenclature for A site $(Na + K) > 0.50$, $Ti < 0.50$, $Fe^{+3} < Al^{vi}$, whereas those in italic type refer to nomenclature for A site $(Na + K) > 0.50$, $Ti < 0.50$, $Fe^{+3} > total\ Al$.

Biotite

Biotite is exclusively found in dacitic and rhyolitic lavas and dikes from Sepulcher Mountain. It is present in all intrusive rocks from Electric Peak. Texturally, biotite occurs as anhedral shreds to euhedral sheets. In intrusive rocks biotite is often uniquely associated with opaque minerals in crystal clots and it often replaces amphibole. Biotite occasionally contains metamict zircon in silicic intrusive rocks.

Fe-Ti Oxides

Oxide minerals are present as microphenocrysts in all rocks from the EPSM complex. Analyses of opaque minerals in extrusive rocks with the electron microprobe suggest that the majority of these opaque minerals are magnetite and ilmenite. Hand sample inspection of intrusive rocks also identified pyrite and chalcopyrite. Opaque minerals occur both as disseminated grains and as crystals in glomerocrysts and amphibole-biotite-oxide clots.

Representative compositions of magnetite and ilmenite are given in Table 5 and Table 6 respectively. Magnetite in extrusive rocks is relatively homogenous with end-member proportions in the magnetite-ulvospinel solid solution series for all samples ranging from $Mt_{52}Ulv_{48}$ to $Mt_{57}Ulv_{43}$ (Table 5). Ilmenite compositions exhibit more compositional variability than magnetite with end-member proportions in the ilmenite-hematite solid solution series ranging from $Ilm_{54}Hm_{46}$ to $Ilm_{74}Hm_{26}$ for all analyses (Table 6). Ternary end-member proportions of Fe-Ti oxides are illustrated in Figure 19.

Quartz

Quartz is present only in two silicic volcanic rocks but is much more abundant in intrusive rocks. Textural varieties in extrusive rocks include quartz phenocrysts that are embayed or which exhibit non-taxial mantling by plagioclase microlites. Quartz crystals in extrusive rocks are predominately anhedral and interstitial to plagioclase, suggesting later crystallization. In a few instances, larger quartz grains exhibit poikilitic domains enclosing plagioclase and opaque minerals. Embayments into and non-taxial mantling of

Table 5. Representative magnetite compositions.

Sample	SiO ₂	n	TiO ₂	Fe ₂ O ₃	FeO	MnO	MgO	Al ₂ O ₃	V ₂ O ₃	ZnO	Mt range	Mt	Ulv
SM9721	58.38	1	6.11 (-)	52.44 (-)	33.72 (-)	0.5 (-)	1.11 (-)	1.77 (-)	0.36 (-)	0.22 (-)	(-)	54	46
SM9814	63.53	9	6.27 (0.08)	52.90 (0.70)	33.97 (0.25)	0.34 (0.01)	1.63 (0.17)	2.21 (0.02)	0.29 (0.01)	0.11 (0.01)	52 to 55	54	46
SM9740	63.84	4	5.21 (0.10)	56.63 (0.12)	33.00 (0.08)	0.8 (0.02)	1.34 (0.02)	1.94 (0.02)	0.16 (0.01)	0.21 (0.02)	55 to 56	56	44
SM9724	68.43	12	6.19 (0.05)	51.23 (0.21)	34.35 (0.11)	0.44 (0.01)	0.75 (0.02)	1.67 (0.03)	0.31 (0.01)	0.16 (0.01)	53 to 54	53	47
SM9735	68.95	15	4.18 (0.24)	56.78 (0.25)	32.98 (0.17)	0.39 (0.03)	0.78 (0.05)	1.05 (0.05)	0.25 (0.01)	0.19 (0.01)	56 to 57	56	44

Note: (SiO₂) = whole rock silica content; n = number of analyses from which mean and standard deviation were calculated; ferric and ferrous iron calculated by charge balance; endmembers are normalized to 100%; Mt range = range of magnetite proportions observed in all analyses from which representative compositions were calculated; values in parentheses represent one standard deviation of the mean; (-) = not applicable.

Table 6. Representative ilmenite compositions.

Sample	(SiO ₂)	n	TiO ₂	Fe ₂ O ₃	FeO	MnO	MgO	Ilm Range	% Ilm	% Hem
SM9721	58.38	3	32.17 (0.56)	37.30 (0.66)	25.89 (0.40)	0.82 (0.03)	0.82 (0.03)	60 to 62	61	39
SM9814	63.53	5	29.85 (0.43)	42.75 (0.65)	23.51 (0.29)	0.20 (0.02)	1.78 (0.08)	54 to 58	56	44
SM9740	63.84	4	32.28 (0.97)	39.29 (1.81)	25.70 (0.64)	0.56 (0.07)	1.54 (0.13)	56 to 64	60	40
SM9724	68.43	8	34.83 (0.45)	31.01 (0.97)	28.42 (0.97)	0.76 (0.08)	1.28 (0.09)	64 to 71	67	33
SM9735	68.95	16	36.10 (0.68)	32.03 (1.27)	28.33 (0.49)	0.79 (0.04)	1.86 (0.06)	56 to 74	67	33

Note: (SiO₂) = whole rock silica content; n = number of analyses from which mean and standard deviation were calculated; ferric and ferrous iron calculated by charge balance; endmembers are normalized to 100%; Ilm range = range of ilmenite proportions observed in all analyses from which representative compositions were calculated; values in parentheses represent one standard deviation of the mean.

